

Characterization of Cementitiously Stabilized Layers for Use in Pavement Design and Analysis

DETAILS

72 pages | 8.5 x 11 | PAPERBACK

ISBN 978-0-309-30813-7 | DOI 10.17226/22247

AUTHORS

Wen, Haifang; Muhunthan, Balasingam; Wang, Jingan; Li, Xiaojun; Edil, Tuncer; and James M. Tinjum

BUY THIS BOOK

FIND RELATED TITLES

Visit the National Academies Press at NAP.edu and login or register to get:

- Access to free PDF downloads of thousands of scientific reports
- 10% off the price of print titles
- Email or social media notifications of new titles related to your interests
- Special offers and discounts



Distribution, posting, or copying of this PDF is strictly prohibited without written permission of the National Academies Press. (Request Permission) Unless otherwise indicated, all materials in this PDF are copyrighted by the National Academy of Sciences.

NATIONAL COOPERATIVE HIGHWAY RESEARCH PROGRAM

NCHRP REPORT 789

**Characterization of
Cementitiously Stabilized
Layers for Use in Pavement
Design and Analysis**

**Haifang Wen
Balasingam Muhunthan
Jingan Wang
Xiaojun Li**

WASHINGTON STATE UNIVERSITY
Pullman, WA

**Tuncer Edil
James M. Tinjum**

UNIVERSITY OF WISCONSIN AT MADISON
Madison, WI

Subscriber Categories

Geotechnology • Pavements

Research sponsored by the American Association of State Highway and Transportation Officials
in cooperation with the Federal Highway Administration

TRANSPORTATION RESEARCH BOARD

WASHINGTON, D.C.

2014

www.TRB.org

NATIONAL COOPERATIVE HIGHWAY RESEARCH PROGRAM

Systematic, well-designed research provides the most effective approach to the solution of many problems facing highway administrators and engineers. Often, highway problems are of local interest and can best be studied by highway departments individually or in cooperation with their state universities and others. However, the accelerating growth of highway transportation develops increasingly complex problems of wide interest to highway authorities. These problems are best studied through a coordinated program of cooperative research.

In recognition of these needs, the highway administrators of the American Association of State Highway and Transportation Officials initiated in 1962 an objective national highway research program employing modern scientific techniques. This program is supported on a continuing basis by funds from participating member states of the Association and it receives the full cooperation and support of the Federal Highway Administration, United States Department of Transportation.

The Transportation Research Board of the National Academies was requested by the Association to administer the research program because of the Board's recognized objectivity and understanding of modern research practices. The Board is uniquely suited for this purpose as it maintains an extensive committee structure from which authorities on any highway transportation subject may be drawn; it possesses avenues of communications and cooperation with federal, state and local governmental agencies, universities, and industry; its relationship to the National Research Council is an insurance of objectivity; it maintains a full-time research correlation staff of specialists in highway transportation matters to bring the findings of research directly to those who are in a position to use them.

The program is developed on the basis of research needs identified by chief administrators of the highway and transportation departments and by committees of AASHTO. Each year, specific areas of research needs to be included in the program are proposed to the National Research Council and the Board by the American Association of State Highway and Transportation Officials. Research projects to fulfill these needs are defined by the Board, and qualified research agencies are selected from those that have submitted proposals. Administration and surveillance of research contracts are the responsibilities of the National Research Council and the Transportation Research Board.

The needs for highway research are many, and the National Cooperative Highway Research Program can make significant contributions to the solution of highway transportation problems of mutual concern to many responsible groups. The program, however, is intended to complement rather than to substitute for or duplicate other highway research programs.

NCHRP REPORT 789

Project 4-36
ISSN 0077-5614
ISBN 978-0-309-30813-7
Library of Congress Control Number 2014953276

© 2014 National Academy of Sciences. All rights reserved.

COPYRIGHT INFORMATION

Authors herein are responsible for the authenticity of their materials and for obtaining written permissions from publishers or persons who own the copyright to any previously published or copyrighted material used herein.

Cooperative Research Programs (CRP) grants permission to reproduce material in this publication for classroom and not-for-profit purposes. Permission is given with the understanding that none of the material will be used to imply TRB, AASHTO, FAA, FHWA, FMCSA, FTA, or Transit Development Corporation endorsement of a particular product, method, or practice. It is expected that those reproducing the material in this document for educational and not-for-profit uses will give appropriate acknowledgment of the source of any reprinted or reproduced material. For other uses of the material, request permission from CRP.

NOTICE

The project that is the subject of this report was a part of the National Cooperative Highway Research Program, conducted by the Transportation Research Board with the approval of the Governing Board of the National Research Council.

The members of the technical panel selected to monitor this project and to review this report were chosen for their special competencies and with regard for appropriate balance. The report was reviewed by the technical panel and accepted for publication according to procedures established and overseen by the Transportation Research Board and approved by the Governing Board of the National Research Council.

The opinions and conclusions expressed or implied in this report are those of the researchers who performed the research and are not necessarily those of the Transportation Research Board, the National Research Council, or the program sponsors.

The Transportation Research Board of the National Academies, the National Research Council, and the sponsors of the National Cooperative Highway Research Program do not endorse products or manufacturers. Trade or manufacturers' names appear herein solely because they are considered essential to the object of the report.

Published reports of the

NATIONAL COOPERATIVE HIGHWAY RESEARCH PROGRAM

are available from:

Transportation Research Board
Business Office
500 Fifth Street, NW
Washington, DC 20001

and can be ordered through the Internet at:

<http://www.national-academies.org/trb/bookstore>

Printed in the United States of America

THE NATIONAL ACADEMIES

Advisers to the Nation on Science, Engineering, and Medicine

The **National Academy of Sciences** is a private, nonprofit, self-perpetuating society of distinguished scholars engaged in scientific and engineering research, dedicated to the furtherance of science and technology and to their use for the general welfare. Upon the authority of the charter granted to it by the Congress in 1863, the Academy has a mandate that requires it to advise the federal government on scientific and technical matters. Dr. Ralph J. Cicerone is president of the National Academy of Sciences.

The **National Academy of Engineering** was established in 1964, under the charter of the National Academy of Sciences, as a parallel organization of outstanding engineers. It is autonomous in its administration and in the selection of its members, sharing with the National Academy of Sciences the responsibility for advising the federal government. The National Academy of Engineering also sponsors engineering programs aimed at meeting national needs, encourages education and research, and recognizes the superior achievements of engineers. Dr. C. D. Mote, Jr., is president of the National Academy of Engineering.

The **Institute of Medicine** was established in 1970 by the National Academy of Sciences to secure the services of eminent members of appropriate professions in the examination of policy matters pertaining to the health of the public. The Institute acts under the responsibility given to the National Academy of Sciences by its congressional charter to be an adviser to the federal government and, upon its own initiative, to identify issues of medical care, research, and education. Dr. Victor J. Dzau is president of the Institute of Medicine.

The **National Research Council** was organized by the National Academy of Sciences in 1916 to associate the broad community of science and technology with the Academy's purposes of furthering knowledge and advising the federal government. Functioning in accordance with general policies determined by the Academy, the Council has become the principal operating agency of both the National Academy of Sciences and the National Academy of Engineering in providing services to the government, the public, and the scientific and engineering communities. The Council is administered jointly by both Academies and the Institute of Medicine. Dr. Ralph J. Cicerone and Dr. C. D. Mote, Jr., are chair and vice chair, respectively, of the National Research Council.

The **Transportation Research Board** is one of six major divisions of the National Research Council. The mission of the Transportation Research Board is to provide leadership in transportation innovation and progress through research and information exchange, conducted within a setting that is objective, interdisciplinary, and multimodal. The Board's varied activities annually engage about 7,000 engineers, scientists, and other transportation researchers and practitioners from the public and private sectors and academia, all of whom contribute their expertise in the public interest. The program is supported by state transportation departments, federal agencies including the component administrations of the U.S. Department of Transportation, and other organizations and individuals interested in the development of transportation. **www.TRB.org**

www.national-academies.org

COOPERATIVE RESEARCH PROGRAMS

CRP STAFF FOR NCHRP REPORT 789

Christopher W. Jenks, *Director, Cooperative Research Programs*
Christopher Hedges, *Manager, National Cooperative Highway Research Program*
Amir N. Hanna, *Senior Program Officer*
Andréa Parker, *Senior Program Assistant*
Eileen P. Delaney, *Director of Publications*
Natalie Barnes, *Senior Editor*

NCHRP PROJECT 04-36 PANEL

Field of Materials and Construction—Area of General Materials

Jeff Uhlmeier, *Washington State DOT, Tumwater, WA (Chair)*
Njoroge W. Wainaina, *Geosyntec (formerly North Carolina DOT), Raleigh, NC*
Khaled A. Galal, *ERI, Riyadh, Saudi Arabia*
Georgene M. Geary, *Georgia DOT, Forest Park, GA*
Andrew Gisi, *Kansas DOT, Topeka, KS (retired)*
M. Makbul Hossain, *New York State DOT, Albany, NY*
Jorge A. Prozzi, *University of Texas–Austin, Austin, TX*
Susan L. Tighe, *University of Waterloo, Waterloo, ON*
Jim Sherwood, *FHWA Liaison*
G. P. Jayaprakash, *TRB Liaison*

AUTHOR ACKNOWLEDGMENTS

The research reported herein was performed under NCHRP Project 4-36 by the Washington State University and University of Wisconsin at Madison. The Washington State University was the contractor for this study; the University of Wisconsin served as a subcontractor. Dr. Haifang Wen, Washington State University, was the principal investigator; all work was done under his supervision. The work at University of Wisconsin at Madison was done under the supervision of Dr. Tuncer Edil. Dr. Wen and Dr. Edil would like to acknowledge the efforts of Dr. Ahmet Gocke, Mr. Zhipeng Su, Mr. Tirupan Mandal, and Mr. Jefferey D. Casmer in the sample preparation and testing and other aspects of the experimental work performed in this research.

FOREWORD

By Amir N. Hanna

Staff Officer

Transportation Research Board

This report presents information on the characterization of cementitiously stabilized layers and the properties that influence pavement performance. It also contains recommended performance-related procedures for characterizing these layers and performance-prediction models for incorporation into the mechanistic-empirical pavement analysis methods. The material contained in the report will be of immediate interest to state materials, pavement, and construction engineers and others involved in the different aspects of pavement design and construction.

Cementitiously stabilized materials—such as lean concrete, cement-stabilized aggregate, and soil stabilized with cement, lime, fly ash, or combinations thereof—are often used in subgrade, subbase, and base layers of flexible and rigid pavement structures. The short- and long-term properties of these materials differ substantially depending on factors such as the type and quantity of stabilizing agent, pavement structure, environmental conditions during and after construction, and loading. Although such stabilized materials have been used in highway construction for many years, limited research has dealt with the relationship of the properties of these materials to the performance of the pavements in which they are used. The AASHTOWare Pavement ME Design (formerly DARWin-ME) and the AASHTO *Mechanistic-Empirical Pavement Design Guide Manual of Practice* (MEPDG) provide a methodology for the analysis and performance prediction of pavements incorporating such layers but do not adequately address the characterization of these materials, the changes of their properties over time, and their distress models. In addition, limited material properties have been considered in the MEPDG; other properties may have significant influence on the long-term performance and need to be considered. Thus, research was needed to identify properties of cementitiously stabilized materials that significantly influence the design, constructibility, and performance of highway pavements; to recommend methods for measuring these properties; and to develop performance-prediction models for incorporation into the MEPDG. This information allows for rational analysis and design of flexible and rigid pavements constructed with cementitiously stabilized layers.

Under NCHRP Project 4-36, “Characterization of Cementitiously Stabilized Layers for Use in Pavement Design and Analysis,” Washington State University of Pullman, Washington, worked with the objective of recommending performance-related procedures for characterizing cementitiously stabilized pavement layers for use in pavement design and analysis and incorporation in the MEPDG. To accomplish this objective, the research reviewed available information on the characterization of cementitiously stabilized layers, identified the properties that influence pavement performance and should be considered in pavement design and analysis, proposed test methods for measuring those properties for which test

methods are not readily available, and conducted an experimental investigation to quantify the influence of these properties on performance.

Based on the findings of this work, the research proposed (1) performance models for incorporation into the mechanistic–empirical pavement analysis methods, and possibly the MEPDG, and (2) test methods for measuring several relevant material properties of cementitiously stabilized materials (presented as an attachment to the report) to allow better consideration of cementitiously stabilized layers in pavement structures. The recommended performance models would be particularly useful in improving the performance-prediction ability of the mechanistic–empirical pavement design and analysis procedures and the recommended test methods will facilitate measuring those material properties and their use as inputs into the design and analysis procedures.

Appendixes A through F contained in the research agency’s final report provide elaborations and detail on several aspects of the research; they are not published herein but are available by searching for *NCHRP Report 789* on the TRB website (www.trb.org). These appendixes are:

- A. Literature Review and Survey Results
- B. Mix Design and Test Procedure Evaluation
- C. Development of Experiments and Findings for Distress Models
- D. FWD Backcalculation Error Analysis
- E. Reasonableness Analysis of Field-Calibrated Models
- F. Bibliography

C O N T E N T S

1	Summary
3	Chapter 1 Introduction
3	Background
3	Research Objective
3	Organization of Report
4	Chapter 2 Pavement Distresses
4	Distresses of Hot-Mix Asphalt Pavement
5	Distresses of Concrete Pavements
7	Chapter 3 Laboratory Tests and Model Development
7	Materials and Mixture Design
8	Tests and Model Development
19	Chapter 4 Model Calibration
19	Data for Model Calibration
21	Calibration Procedures
23	Calibration Results
26	Chapter 5 Findings and Recommendations for Research
26	Findings
30	Recommendations for Future Research
31	References
33	Attachment Proposed Test Methods
72	Appendixes

Note: Photographs, figures, and tables in this report may have been converted from color to grayscale for printing. The electronic version of the report (posted on the web at www.trb.org) retains the color versions.

SUMMARY

Characterization of Cementitiously Stabilized Layers for Use in Pavement Design and Analysis

Cementitiously stabilized materials (CSM) have been used extensively by highway agencies over the years. The characterization of CSM, the changes of their properties over time, and their distress models have not been addressed adequately in the *Mechanistic–Empirical Pavement Design Guide* (MEPDG). Research was needed to identify the properties of CSM that significantly affect the design, constructability, and performance of highway pavements and to recommend methods for measuring these properties. This information can be incorporated into the MEPDG to allow rational analysis and design procedures for flexible and rigid pavements that are constructed with cementitiously stabilized layers (CSL). The research performed under NCHRP Project 4-36 provided this information through a review of relevant literature, evaluation of test procedures, and development and calibration of models.

The literature review revealed that shrinkage, fatigue, durability, erosion, strength, and stiffness are properties that greatly affect pavement performance. Performance issues associated with the use of CSL in asphalt pavements include block cracking, transverse cracking, longitudinal cracking, bottom-up cracking (alligator cracking), rutting, and heave. Cracking and faulting are the primary distress types found in concrete pavement. Also, the literature review identified the models that consider the effects of such factors as repeated loading and the environment on the different distress types.

The test procedures that are currently used for measuring performance-related properties were assessed in terms of their performance predictability, precision, accuracy, practicality, cost, and test time. Also, potential new test procedures or modifications to current test procedures were proposed for measuring those properties for which no suitable test method was available. These new or modified procedures were evaluated in the laboratory and, as a result, test methods for measuring the unconfined compressive strength (UCS), the modulus of rupture (MOR), and the indirect tensile (IDT) strength were proposed. Flexural modulus and resilient modulus were proposed for both heavily and lightly stabilized materials, respectively. Laboratory beam fatigue testing was recommended for developing fatigue models, and wet-dry and freeze-thaw tests were recommended for developing durability models. A suite of shrinkage-related tests were performed and used to develop models for free-drying shrinkage (including ultimate drying shrinkage), coefficient of thermal expansion, coefficient of friction, and restrained shrinkage cracking. Cyclic impact erosion testing was recommended for erosion model development.

Once the appropriate test procedures were identified, a laboratory investigation was performed and performance-related models were developed for modulus and strength growth, durability, fatigue, shrinkage cracking, and erosion. The growth models were developed from tests on specimens that were conditioned at different temperatures and humidity for up to 360 days to allow consideration of the effect of temperature and humidity conditions on the

IDT strength and modulus values and their contribution to early-age shrinkage cracking. Bottom-up fatigue models were developed from tests on CSM beams subjected to repeated loads representing specific stress ratios. Durability models were developed based on the CSM degradation measured in wet–dry and freeze–thaw tests. A model that combines top-down compressive fatigue and erosion was developed from cyclic impact tests conducted on CSM specimens submerged in water to simulate the impact of traffic loading and water movement. Shrinkage cracking models were developed from restrained shrinkage cracking tests on beam specimens.

The models developed based on laboratory tests were then calibrated using data from field measurements and the MEPDG software. First, traffic, climate, and material properties were used as inputs to the MEPDG analysis procedure, and the properties of all layers (except CSL) during the course of the pavement life were determined. These properties included the modulus (with the aging effect) of the asphalt layer and the resilient modulus (with the moisture variation effect) of each unbound layer. The CSL properties and the MEPDG-provided layer properties were used as inputs to a linear elastic layered program developed by the research team to determine the pavement responses on a monthly basis. The increase of the modulus value over time and the degradation of the modulus due to wet–dry and freeze–thaw cycles were considered for each month. These responses were then used as inputs to the fatigue and erosion models in which the initial values of the model parameters were used. The fatigue lives of CSL were computed, and the damage due to traffic was determined on a monthly basis. The degradation of the moduli of the CSL over time were determined and compared with those backcalculated from falling weight deflectometer (FWD) test results; regression analyses provided the calibrated model parameters. Because available models do not accurately predict crack spacing and width, shrinkage crack spacing and width models were developed based on dimensional analysis, using data from field measurements.

The performance models developed in this research could possibly be incorporated into the MEPDG to improve consideration of CSL. Also, the new test methods proposed for measuring certain CSM properties seem appropriate for AASHTO consideration as standard test methods. In addition, several research topics have been identified based on the findings of the research; these seem to warrant consideration.

CHAPTER 1

Introduction

Background

The use of cementitiously stabilized materials (CSM)—such as lean concrete; cement-stabilized aggregate; and soil stabilized with cement, lime, fly ash, or combinations thereof in the subgrade, subbase, and base layers of flexible and rigid pavement structures—is a widely accepted practice by many state highway agencies. Although a substantial amount of research has been undertaken to study the properties of these materials, very little research has been conducted that relates the properties of such materials to the performance of the pavements in which they are used. The AASHTOWare Pavement ME Design (formerly DARWin-ME), which is based on the *Guide for Mechanistic–Empirical Design of New and Rehabilitated Permanent Structures* (ARA 2004), provides a methodology for the analysis and performance prediction of pavements that incorporate such layers. However, the properties of these materials change substantially over time (in short and long terms) depending on the type and quantity of the stabilizing agent, pavement structure, environmental conditions during and after construction, and traffic loading. The characterization of such materials, the changes of their properties over time, and their performance models have not been addressed adequately in the *Mechanistic–Empirical Pavement Design Guide* (MEPDG). Those properties that may have a significant effect on the long-term performance of pavements need to be considered.

Thus, research was needed to identify the properties of CSM that significantly affect the design, constructability, and performance of highway pavements and to recommend methods for measuring these properties. This information can then be incorporated into the MEPDG to allow for the rational analysis

and development of design procedures for pavements constructed with stabilized layers. NCHRP Project 4-36 was initiated to address this need.

Research Objective

The objective of this research was to recommend performance-related procedures for characterizing cementitiously stabilized layers (CSL) for use in pavement design and analysis and incorporation into the MEPDG. This research addressed material properties and related test methods that can be incorporated in the pavement design and analysis procedures to predict pavement performance. This research dealt with subgrade, subbase, and/or base materials that have been stabilized with hydraulic cement, fly ash, lime, or combinations thereof and used in pavements.

Organization of Report

This report consists of five chapters. This chapter presents the background and research objective. Chapter 2 presents the findings from the literature review. Chapter 3 summarizes the laboratory tests and model development. Chapter 4 presents the results of the model calibration based on the collected field data. Chapter 5 provides findings and recommendations for future research. An attachment to the report contains several methods of test that are proposed for consideration and adoption by AASHTO. Six appendixes (A through F), not published herein but available on the TRB website by searching for *NCHRP Report 789*, provide further elaboration on the research.

CHAPTER 2

Pavement Distresses

This chapter summarizes the findings from the literature review regarding the distresses of asphalt and concrete pavements built with CSL and the properties of CSM that contribute to these distresses (details are provided in Appendix A).

Distresses of Hot-Mix Asphalt Pavements

Block Cracking in Hot-Mix Asphalt

Block cracking often is reported in hot-mix asphalt (HMA) pavements with CSL. This cracking is caused by shrinkage of the underlying stabilized base (Scullion 2002) that results from the loss of moisture and temperature variation. The shrinkage typically occurs shortly after construction and continues thereafter. Also, block cracking occurs in CSM with high unconfined compressive strength (UCS) (Zube et al. 1969), likely due to the high shrinkage caused by the high binder content generally used in these materials.

Transverse Cracking

Some of the transverse cracking in the HMA surface layer results from the shrinkage of the stabilized base (Atkinson 1990, Chen 2007). This cracking starts from the bottom of the surface layer and propagates through the surface layer. Such cracking also can be due to the low bond between the surface layer and the stabilized base (George 2002). Transverse cracking in pavements with a granular base and a stabilized subbase does not occur until later in the life of the pavement (Ramsey and Lund 1959). Shrinkage cracking of the subbase causes stress concentrations at the crack locations and eventually affects the stress distribution in the surface layer. The survey results (presented in Appendix A) indicate that state agencies consider transverse and block cracking to be the most severe distress types in pavements constructed with CSL.

Longitudinal Cracking

CSL provide strong support to HMA surface layer that reduces tension at the bottom of the surface layer and helps reduce bottom-up fatigue of the surface layer. Thus, use of a stabilized base will reduce alligator cracking in HMA. However, the HMA surface layer of asphalt pavements with high stiffness CSL as the base is prone to top-down fatigue cracking in the wheel-path (ARA 2004, Scullion et al. 2003). This fatigue cracking is due to the high shear/tension at the surface of the HMA contributed by the high stiffness of the CSL.

Dry-land longitudinal cracking outside the wheel-path has also been reported for pavements with CSL but it is generally caused by the shrinkage of expansive soils and not by CSL (Luo and Prozzi 2008, Wise and Hudson 1971, Syed et al. 2000, Chen 2007, Atkinson 1990). This type of cracking is not considered in this research.

Bottom-up Cracking (Alligator Cracking) of HMA Layer

Bottom-up cracking may occur due to erosion or fatigue of the CSL as described in the following list:

- Erosion of the surface of the stabilized base layer can create a layer of loose material between the HMA and the CSL at the base (Li et al. 1999, Meng et al. 2004, Thogersen and Bjulf 2005). This erosion increases the strain level at the bottom of the HMA layer leading to alligator cracking. In addition, the loss of fines in the loose material generated by the erosion of the stabilized materials may cause pumping (De Beer 1985).
- Alligator cracking in HMA pavements can be induced by fatigue cracking of the stabilized base or subbase due to repeated traffic loads (Pretorius and Monismith 1972, Scullion and Harris 1998, Li et al. 1999). Under these loads, microcracks are initiated at the bottom of the CSL

due to tensile stress/strain and then propagate upwards. The fatigue of CSL leads to a decrease in the modulus values of the CSL thereby increasing the tensile strain at the bottom of the HMA layer and causing fatigue cracking in the HMA layer. When a CSL is subjected to freeze–thaw and/or wet–dry cycling, the modulus value and strength are reduced and, consequently, the fatigue resistance is also reduced (Naji and Zaman 2005).

- The rutting potential in asphalt pavements with CSL is reduced because of the relatively high stiffness of CSL (Von Quintus et al. 2005). However, rutting in the asphalt layer may occur because of the resulting high shear stress in the HMA layer, the erosion of the CSL, or the failure of the CSL as described below:
 - Rutting induced by high shear stress—The high stiffness of the CSL influences the stress/strain state distribution such that shear strain may occur in the HMA layer, increasing the potential for HMA rutting (Meng et al. 2004, Bonnot 1991).
 - Rutting induced by erosion—Erosion of the CSL results from repeated shear stress caused by the water movement that occurs due to repeated traffic loads (De Beer 1985). Also the fines in CSL could become detached and form a soft layer between the CSL and upper layer (Metcalf et al. 2001). When cracks occur, the fines can be pumped out of the pavement through the cracks leading to a soft layer and/or voids that contribute to rutting in the asphalt pavement.
 - Rutting induced by fatigue failure—For thick CSL, compression/crushing fatigue of the CSL could result from repeated compression at the top of CSL. For such layers, the tensile strain at the bottom of the CSL is too small to cause tensile fatigue, but the compressive strain is so high that it causes crushing in the top 2 to 3 in., especially in the presence of excessive moisture (De Beer 1990). An increase in the UCS of CSM reduces the compression strain and increases the crushing fatigue life

(Theyse et al. 1996). A compressive strain of 1% has been suggested as the failure strain for compression fatigue. Top-down compressive fatigue often occurs when a thin asphalt layer is placed on top of a lightly stabilized, thick layer.

Heave

The swelling of expansive soils can cause heaving in the pavement; expansive soil often is stabilized to mitigate such swelling. However, the use of calcium-based binder for soils with high sulfate concentration leads to ettringite formation that causes a significant volume change when hydrated (Chen et al. 2005, Si 2008, Little and Nair 2007) and heaving in the asphalt pavement. Expansive soils are generally removed and replaced with non-expansive soils; therefore, swelling is not addressed in this research.

Distresses of Concrete Pavements

Numerous studies have indicated the contributions of stabilized base layers to reduced faulting, pumping, and cracking of concrete pavements (ARA 2004, Selezneva et al. 2000, Nussbaum and Childs 1975, Neal and Woodstrom 1977, Ruiz et al. 2005). However, shrinkage cracking of CSL and the bond between the concrete layer and stabilized base could contribute to early-stage cracking of concrete pavement (Mallela et al. 2007).

Erosion of CSL also contributes to cracking and joint faulting in concrete pavements. Pumping of fines leads to voids underneath the concrete slab under repeated traffic loads, resulting in stress concentrations and cracking. The movement of the loosened materials from one joint side to the other may cause joint faulting (Jung et al. 2009, ARA 2004).

Table 2-1 provides a summary of the relationship of CSL properties to the distress in asphalt and concrete pavements.

Table 2-1. Relationship of CSL properties to pavement distress.

Pavement Distress	CSL Property						
	Stiffness/Modulus	Strength	Durability (freeze-thaw, wet-dry)	Fatigue Resistance	Erodibility Resistance	Shrinkage Resistance	Swell Resistance
Rutting in Asphalt Layer	(+) CSL Base	(+) CSL Base		(-) CSL Base	(-) CSL Base		
Block Cracking in Asphalt Layer						(-) CSL Base	
Bottom-Up Alligator Cracking of Asphalt Layer	(-) CSL Base/Subbase	(-) CSL Base	(-) CSL Base/Subbase	(-) CSL Base/Subbase	(-) CSL Base		
Transverse Cracking in Asphalt Layer						(-) CSL Base	
Top-Down Longitudinal Cracking in Wheel-Path	(+) CSL Base/Subbase	(+) CSL Base					
Heaving							(-) CSL Base/Subbase
Transverse Cracking of Concrete Pavement					(-) CSL Base	(-) CSL Base	
Faulting of Concrete Pavement					(-) CSL Base		

Note: (+) indicates a positive relationship (e.g., the rutting potential in the asphalt layer increases as the modulus value increases) and (-) indicates a negative relationship.

CHAPTER 3

Laboratory Tests and Model Development

Materials and Mixture Design

Four types of material were used for stabilization in this project: high- and low-plasticity fine-grained soils (clay and silt) and two granular materials (sand and gravel). These materials were characterized in terms of moisture–density relationships, Atterberg limits, and gradation. Figure 3-1 presents the gradations of the four materials and Table 3-1 lists their Atterberg limits and designations.

The binders used were cement, lime, and Class F and Class C fly ash.

Nine mixtures were designed following the procedures developed by the National Lime Association (NLA) for soil–lime (NLA 2006), the Portland Cement Association (PCA) for soil–cement (PCA 1992), and the Federal Highway Administration (FHWA) for soil–fly ash (Veisi et al. 2010) to determine the appropriate binder contents. Table 3-2 lists the type and content of the binder used with each material (details are provided in Appendix B). The clay–lime material was cured at 104°F, and the other eight mixtures were cured at 68°F. These mixtures were used for model development recognizing that the binder content could vary depending on

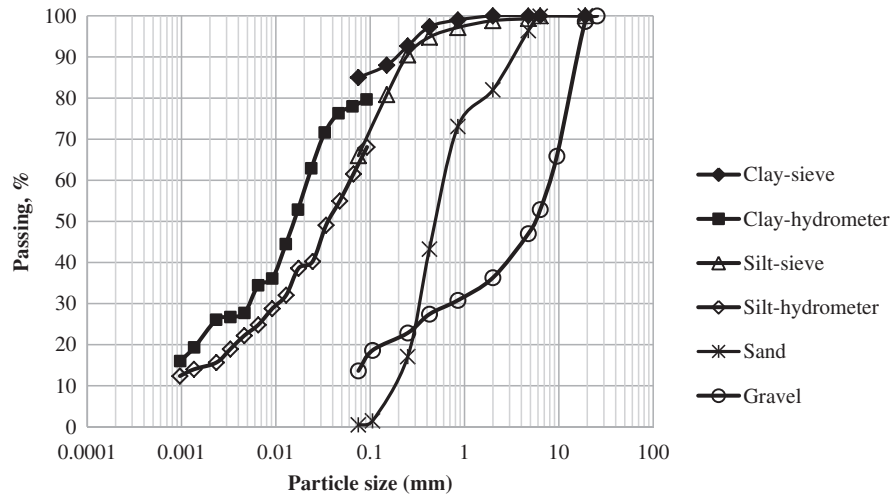


Figure 3-1. Gradation of soils.

Table 3-1. Characteristics of soils.

		Clay	Silt	Sand	Gravel
Atterberg Limit	Liquid Limit (LL)	39	17	–	–
	Plastic Limit (PL)	23	15	–	–
	Plasticity Index (PI)	16	2	–	–
Designation	Unified Soil Classification System (USCS)	CL	ML	SP	GM
	AASHTO	A-6	A-4	A-1-b	A-1-a

Table 3-2. Mix design of stabilized mixtures.

	Clay	Silt	Sand	Gravel
Cement	12%	8%	6%	3%
Lime	6%	4% + 12%*	–	–
Fly Ash C	–	13%	13%	13%

*Class F Fly Ash

the location of the material within the pavement structure (e.g., base or subbase).

Three replicates were used for each UCS test. A 7-day UCS of 200 psi was used as the criterion to distinguish between heavily and lightly stabilized materials (i.e., heavily stabilized materials have a 7-day UCS ≥ 200 psi and lightly stabilized materials have a 7-day UCS < 200 psi). Based on this criterion, clay–lime and silt–C fly ash mixtures were categorized as lightly stabilized and the other seven mixtures were categorized as heavily stabilized materials.

Tests and Model Development

The material properties that influence the pavement performance were identified through the literature review. Also, the test methods for measuring these properties were identified and assessed in terms of performance predictability, precision, accuracy, practicality, and cost. Promising test methods were then evaluated in the laboratory to determine their applicability to CSM (details are provided in Appendix B). Table 3-3 lists the proposed material properties and test procedures; brief descriptions are provided in the following sections.

Modulus/Strength Growth

When cement is used as the binder, high modulus/strength can form fairly quickly. However, early-age modulus/strength development for lime and/or fly ash–stabilized CSM is relatively slow in comparison to that of cement-stabilized CSM but can continue for years due to pozzolanic reactions. The modulus/strength development of CSM was examined; a brief description is provided (details are provided in Appendix C).

Strength

The strength of CSM is characterized by the UCS, indirect tensile (IDT) strength, and modulus of rupture (MOR). The strength gain after 3, 7, 28, 90, 180, and 360 days of curing at 68°F and 100% relative humidity (RH) was measured, with one replicate of each mixture.

The relationships between MOR and UCS and between IDT strength and UCS are illustrated in Figures 3-2 and 3-3 and presented by Equations 3-1 and 3-2, respectively. The relationship between IDT strength and MOR, presented in Equation 3-3, was derived from these two equations. These relationships provide estimates of the strength values that can be used as Level 2 inputs in the MEPDG (ARA 2004).

$$MOR = 0.14 \times UCS \tag{3-1}$$

$$S_{IDT} = 0.12 \times UCS \tag{3-2}$$

$$S_{IDT} = 0.86 \times MOR \tag{3-3}$$

Table 3-3. Material properties and performance tests.

	Environmental Model		Pavement Response Model	Distress Model		
	Freezing and Thawing	Wetting and Drying	Modulus	Bottom-Up Tensile Fatigue	Top-Down Compressive Fatigue-Erosion	Shrinkage Cracking
Material Properties	Strength		<ul style="list-style-type: none"> Flexural modulus for heavily stabilized materials Resilient modulus for lightly stabilized materials 	Modulus of rupture	Unconfined compressive strength	<ul style="list-style-type: none"> Indirect tensile modulus Indirect tensile strength Ultimate drying shrinkage strain Gradient drying shrinkage strain Coefficient of thermal expansion Coefficient of friction
Tests for Model Development or Calibration	Freeze–thaw cycling	Wet–dry cycling	–	Beam fatigue	Cyclic impact erosion	Restrained shrinkage cracking test

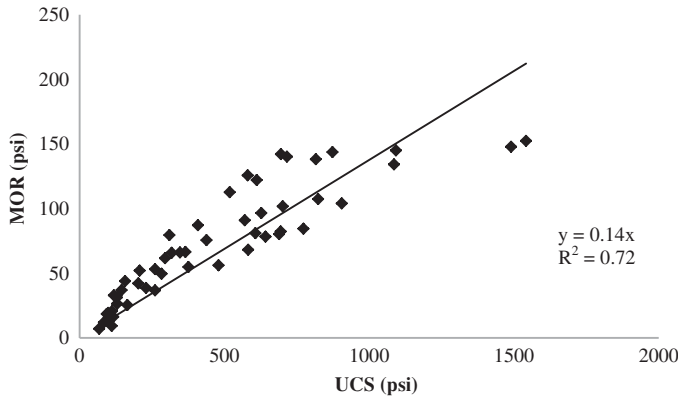


Figure 3-2. Modulus of rupture versus unconfined compressive strength.

where

- MOR = modulus of rupture, psi
- S_{IDT} = indirect tensile strength, psi
- UCS = unconfined compressive strength, psi

Because the 28-day strength is commonly used for quality control and performance prediction, a model based on the 28-day strength was developed to predict the UCS, IDT, or MOR at any age for the 68°F and 100% RH curing condition. The model is presented by Equation 3-4; the measured versus predicted strength is illustrated in Figure 3-4.

$$S_t(t) = (S_{28}) \left[p_1 \left(1 + \frac{1}{\left(1 + \frac{t-t_0}{p_2} \right)} \right) \right] \quad (3-4)$$

where

- $S_t(t)$ = strength (UCS, IDT, or MOR) at age t months, psi
- S_{28} = strength (UCS, IDT, or MOR) after 28 days of curing at 68°F and 100% RH

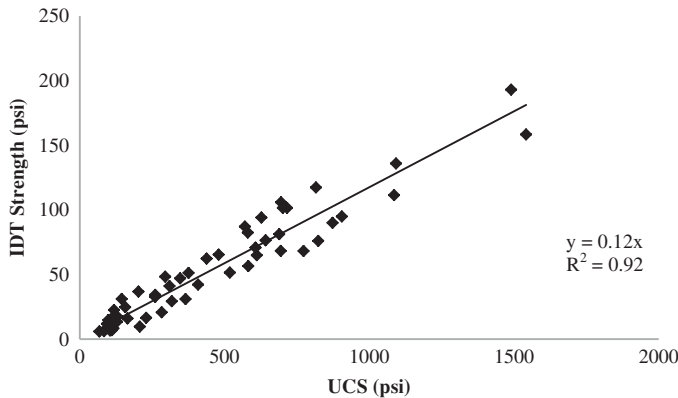


Figure 3-3. Indirect tensile versus unconfined compressive strength.

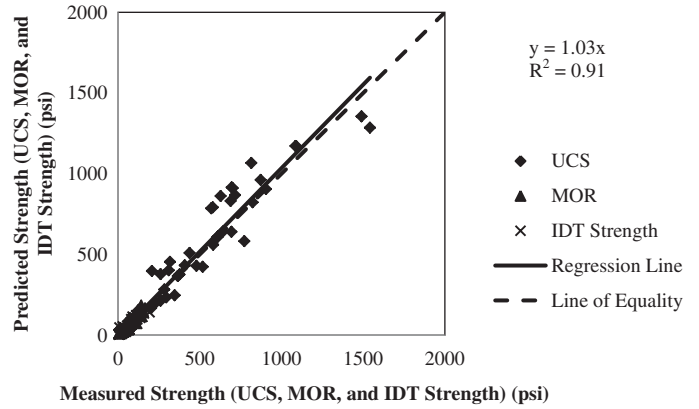


Figure 3-4. Predicted versus measured strength.

- t_0 = time corresponding to S_{28} in months (e.g., 28/30.5 assuming 30.5 days/month)
- p_1, p_2 = regression parameters (1.59 and 1.61, respectively)

Modulus

The relationships between the different types of strength and modulus are illustrated in Figures 3-5 and 3-6 and presented by Equations 3-5 through 3-7. Equation 3-7 was derived from Equations 3-1 and 3-5. These relationships provide estimated values that can be used as Level 2 inputs in the MEPDG.

$$E_f = 936.28 \times \text{MOR} + 62382 \quad (3-5)$$

$$E_t = 7980.1 \times S_{IDT} \quad (3-6)$$

$$E_f = 131.08 \times \text{UCS} + 62382 \quad (3-7)$$

where

- E_f = flexural modulus, psi
- E_t = indirect tensile modulus, psi
- S_{IDT} = indirect tensile strength, psi
- MOR = modulus of rupture, psi

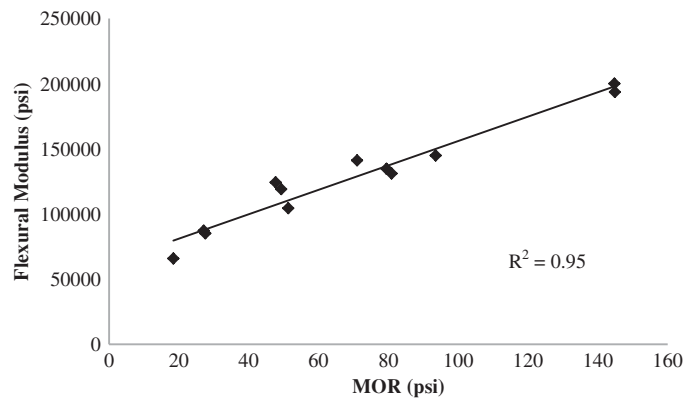


Figure 3-5. Modulus of rupture versus flexural modulus.

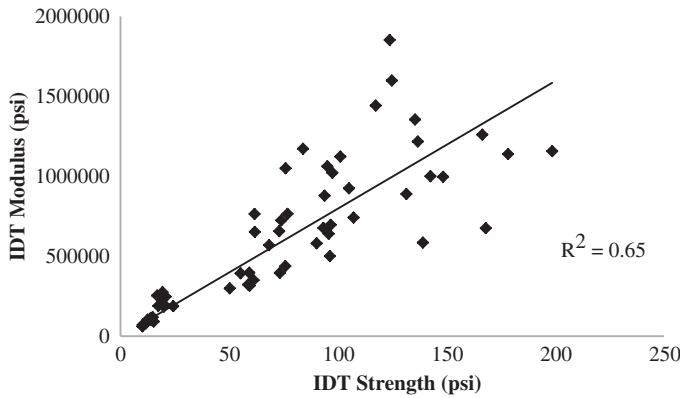


Figure 3-6. IDT strength versus IDT modulus.

The flexural modulus after t months can be derived from Equations 3-4 and 3-7 as follows:

$$E_f = 131.08 \times (\text{UCS}_{28}) \left[p_1 \left(\frac{1}{1 + \frac{(t-t_0)}{p_2}} \right) \right] + 62382 \quad (3-8)$$

The resilient modulus (M_r) for lightly stabilized materials can be estimated from the UCS (ARA 2004) using Equation 3-9.

$$M_r = 0.12 \times \text{UCS} + 9.98 \quad (3-9)$$

where

M_r = resilient modulus, ksi

Similarly, the resilient modulus after t months of curing at 68°F and 100% RH can be estimated from Equation 3-10.

$$M_r = 0.12 \times (\text{UCS}_{28}) \left[p_1 \left(\frac{1}{1 + \frac{(t-t_0)}{p_2}} \right) \right] + 9.98 \quad (3-10)$$

where

UCS_{28} = UCS after 28 days of curing at 68°F and 100% RH

t = time in months corresponding to M_r (assuming each month has 30.5 days)

t_0 = time in months corresponding to UCS_{28} (i.e., 28/30.5)

p_1, p_2 = regression parameters (1.59 and 1.61, respectively).

IDT Strength and Modulus Models Considering Temperature and RH Effects

Shrinkage cracking is influenced by the early-age tensile strength/modulus and the environmental conditions, particularly the temperature and RH. Therefore, models were developed for estimating the IDT strength and modulus val-

ues at various temperatures and RH. These models are presented as Equation 3-11a and 3-11b.

$$S_{\text{IDT}} = p_5 (\text{UCS}_{28}) \left[p_1 \left(\frac{1}{1 + \frac{t-28/30.5}{p_2}} \right) \left(\frac{1 + \frac{\text{RH}}{100}}{2} \right)^{p_3} \left(\frac{T-32}{293.15} + 273.15 \right)^{p_4} \right] \quad (3-11a)$$

$$E_t = q_5 (\text{UCS}_{28}) \left[q_1 \left(\frac{1}{1 + \frac{t-28/30.5}{q_2}} \right) \left(\frac{1 + \frac{\text{RH}}{100}}{2} \right)^{q_3} \left(\frac{T-32}{293.15} + 273.15 \right)^{q_4} \right] \quad (3-11b)$$

where

S_{IDT} = IDT strength at age t months, psi

E_t = IDT modulus at age t months, psi

UCS_{28} = unconfined compressive strength after 28 days of curing at 68°F and 100% RH, psi

t = curing time, months (assuming each month has 30.5 days)

RH = curing relative humidity, %

T = temperature, °F

p_1, p_2, p_3, p_4, p_5 = strength regression parameters (listed in Table 3-4)

q_1, q_2, q_3, q_4, q_5 = modulus regression parameters (listed in Table 3-4)

Figure 3-7 presents a comparison of the measured and predicted IDT strength and modulus values after 3, 7, 14, 28, and 56 days of curing.

Durability

Tests were conducted to determine the effect of wet-dry and freeze-thaw cycles on the UCS; Equation 3-12 presents this effect. Model parameters obtained from the laboratory test results are listed in Table 3-5; a comparison of the measured and predicted UCS values is shown in Figure 3-8.

$$\text{UCS}(N) = \text{UCS}_{\text{current}} \left[\frac{m_1 / \ln(\text{UCS}_{28})}{1 + e^{(m_1 N)}} + 1 - \frac{m_1 / \ln(\text{UCS}_{28})}{2} \right] \quad (3-12)$$

Table 3-4. Parameters for IDT strength/modulus model.

Model	Parameter	1	2	3	4	5
IDT strength	p	1.59	1.61	-1.50	23.41	0.11
IDT modulus	q	1.59	1.61	-0.23	0	1223

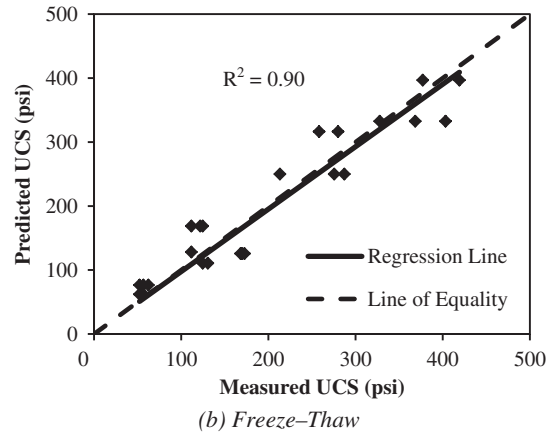
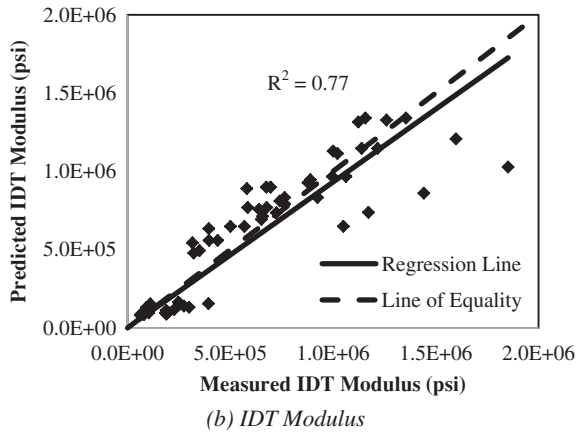
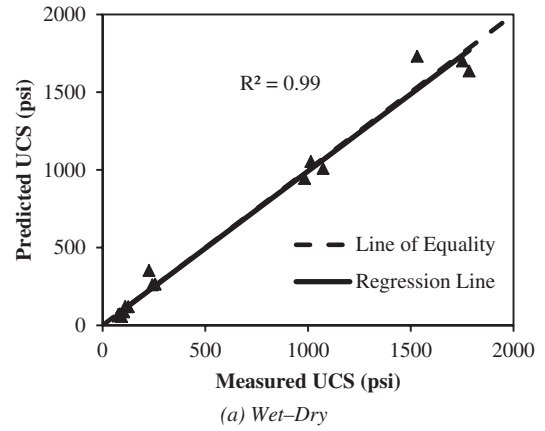
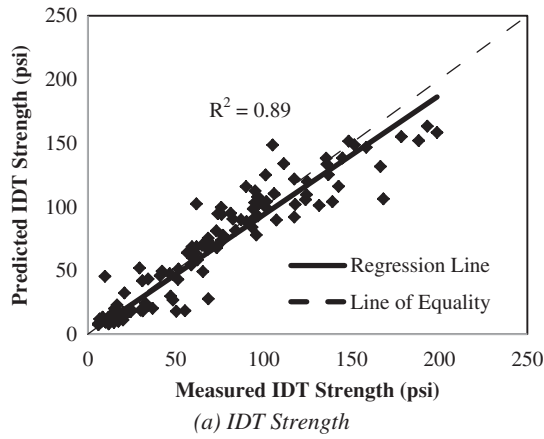


Figure 3-7. Measured versus predicted IDT strength and modulus values.

Figure 3-8. Measured versus predicted UCS values after wet-dry/freeze-thaw cycles.

where

- UCS(*N*) = UCS after *N* cycles of freeze-thaw or wet-dry, psi
- UCS_{current} = UCS before freeze-thaw or wet-dry cycles, psi
- UCS₂₈ = 28-day UCS, psi
- N* = number of freeze-thaw or wet-dry cycles
- m*₁, *n*₁ = model parameters for wet-dry or freeze-thaw durability models

Fatigue

Fatigue of CSL occurs as a result of repeated traffic loads and is categorized as bottom-up tensile fatigue or top-down

Table 3-5. Regression parameters of durability models.

Model	Parameter	Value
Wet-dry	<i>m</i> ₁	2.58
	<i>n</i> ₁	0.62
Freeze-thaw	<i>m</i> ₁	6.68
	<i>n</i> ₁	0.93

compressive fatigue. The fatigue life of CSL typically is related to the ratio of applied stress to strength or the ratio of applied strain to breaking strain (Austroads 2008, ARA 2004, Otte 1978, Sobhan and Das 2007, Yeo 2008). The number of load repetitions that reduces the modulus value to 50% of its initial value is considered the fatigue life (Midgley and Yeo 2008).

Bottom-Up Tensile-Fatigue Test

Beam fatigue tests were conducted on 12 types of materials to determine the bottom-up tensile-fatigue life of CSM. Test results are shown in Figure 3-9 and the stress-based fatigue model is presented by Equation 3-13.

$$\ln(N_{ft}) = k_1 \left(\frac{k_2 - \frac{\sigma_t}{MOR}}{k_3} \right) \quad (3-13)$$

where

- N*_{ft} = bottom-up tensile-fatigue life
- σ_t = tensile stress at the bottom of beam, psi
- MOR = modulus of rupture, psi

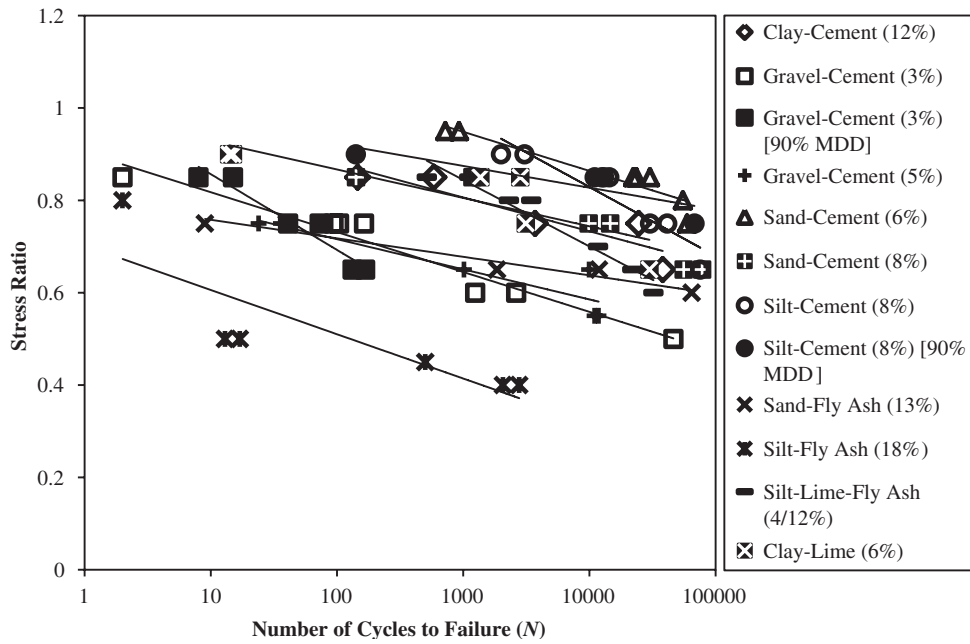


Figure 3-9. Bottom-up tensile-fatigue life versus stress ratio.

k_1 = parameter used for field calibration (1.0 for laboratory tests)

k_2, k_3 = regression parameters

The k_2 and k_3 values for the different materials are listed in Table 3-6.

The accumulated damage and the modulus of the material after experiencing damage can be obtained from Equations 3-14 and 3-15, respectively.

$$D = \sum_{i=1}^j \frac{n_i}{N_i} \quad (3-14)$$

Table 3-6. Parameters of bottom-up tensile-fatigue life model.

Material (Binder Content)	Regression Parameters		R ²
	k_2	k_3	
Clay-Cement (12%)	0.03	1.03	0.82
Gravel-Cement (3%)	0.04	0.90	0.95
Sand-Cement (6%)	0.04	1.20	0.88
Silt-Cement (8%)	0.06	1.43	0.87
Sand-Fly Ash (13%)	0.02	0.80	0.95
Silt-Lime-Fly Ash (4%/12%)	0.06	1.28	0.94
Clay-Lime (6%)	0.03	0.99	0.72
Gravel-Cement (3%) [90% MDD]	0.07	1.02	0.93
Silt-Cement (8%) [90% MDD]	0.02	1.02	0.74
Gravel-Cement (5%)	0.03	0.85	0.89
Sand-Cement (8%)	0.03	1.06	0.89
Silt-Fly Ash (18%)	0.04	0.70	0.70
Average	0.04	1.02	-

$$E(D) = E_{\text{current}} \left[\frac{m_2 / \ln(\text{UCS}_{28})}{1 + e^{\sinh(n_2 D)}} + 1 - \frac{m_2 / \ln(\text{UCS}_{28})}{2} \right] \quad (3-15)$$

where

D = accumulated damage

j = total number of load groups

n_i = number of repetitions of load group i

N_i = number of repetitions to fatigue of load group i

$E(D)$ = modulus after accumulated damage D

UCS_{28} = 28-day unconfined compressive strength, psi

E_{current} = modulus before fatigue damage at age t in months, psi

m_2 and n_2 = regression parameters for bottom-up tensile fatigue or top-down compressive-fatigue and erosion models.

Top-Down Compressive-Fatigue and Erosion Test

The combined effect of moisture and top compressive strain significantly accelerates top-down compressive-fatigue failure (De Beer 1990). A model that combines top-down compressive fatigue and erosion was developed. The pressure from traffic saturates and weakens the CSM, making it prone to top-down compressive fatigue. The compressive stress from traffic detaches the particles, and then shear stress caused by water movement under traffic transports the particles and leads to erosion. The cyclic impact erosion (CIE) test developed by Sha and Hu (2002), shown schematically in Figure 3-10, simulates CSL erosion and top-down compressive fatigue in the field. Controlled-displacement tests were conducted on specimens submerged in water. When the vertical load impacts the

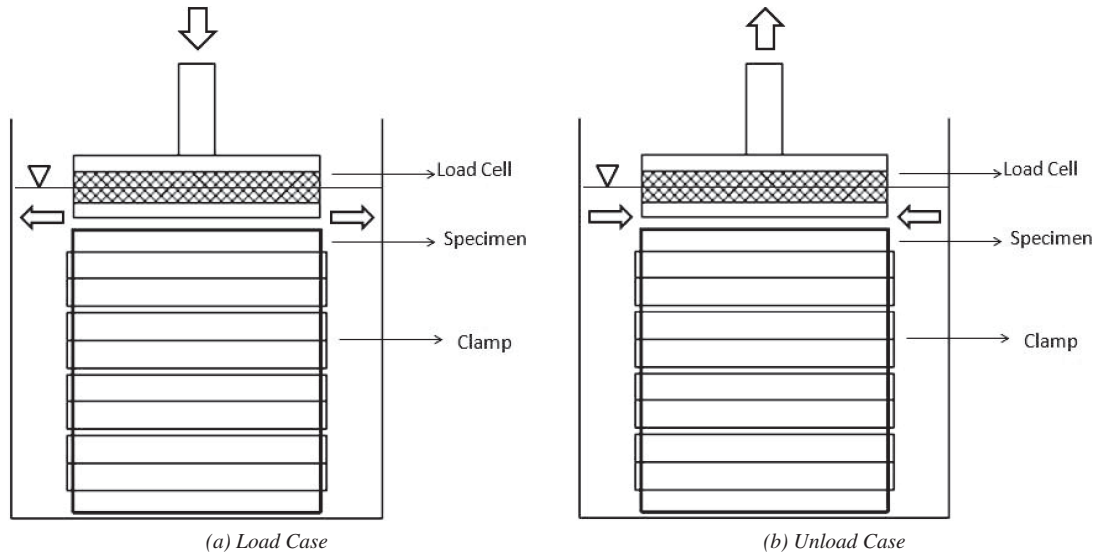


Figure 3-10. Schematic view of CIE test setup.

sample surface, the particles detach from the specimen causing the load to decrease; the modulus is also decreased.

The top-down compressive-fatigue-erosion life is calculated from Equation 3-16.

$$\log N_{fc} = k_4 \log \left(\frac{\rho}{\omega} \right) \left(1 - \frac{\sigma_c}{k_5 \text{UCS}} \right) \quad (3-16)$$

where

N_{fc} = top-down compressive-fatigue-erosion life (defined as the number of cycles that reduce the modulus to 50% of its initial value)

ρ = maximum dry density, lb/ft³

ω = optimum moisture content, %

σ_c = compressive stress applied on the top of specimen, psi

UCS = current unconfined compressive strength, psi

k_4, k_5 = regression parameters

After the top-down compressive-fatigue-erosion life is estimated, the damage and the reduced modulus can be calculated using Equations 3-14 and 3-15, respectively. Table 3-7 lists the model parameters and Figures 3-11 and 3-12 present comparisons of the measured and predicted fatigue life and modulus values, respectively.

Table 3-7. Parameters for top-down compressive-fatigue-erosion model.

Model	Parameter	
Top-Down Compressive-Fatigue-Erosion Fatigue Life	k_4	2.79
	k_5	3.39
Top-Down Compressive-Fatigue-Erosion Modulus Reduction	m_2	6.77
	n_2	1.99

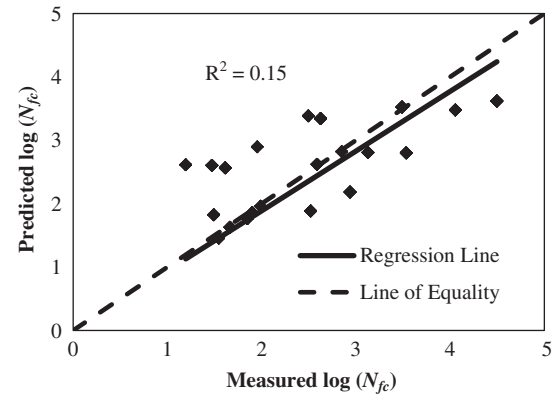


Figure 3-11. Measured versus predicted fatigue life values for top-down compressive-fatigue-erosion model.

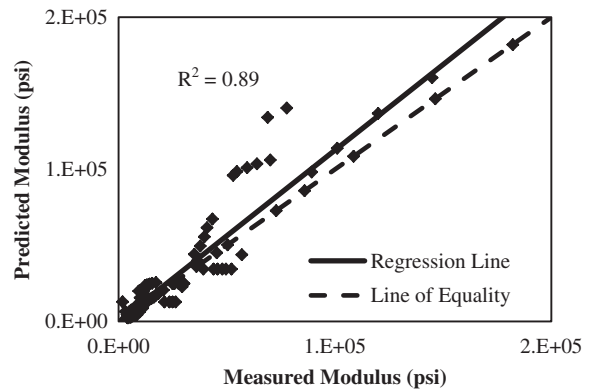


Figure 3-12. Measured versus predicted modulus values for top-down compressive-fatigue-erosion model.

Shrinkage

Shrinkage cracking test sets were conducted on clay–cement, silt–cement, and clay–lime at various combinations of RH and temperatures (68°F and 65% RH, 68°F and 40% RH, and 104°F and 40% RH). Each set included tests for determining the coefficient of thermal expansion (COTE), ultimate drying shrinkage strain, drying shrinkage strain gradient, large-scale restrained shrinkage cracking (using epoxy as the bonding agent), coefficient of friction, and IDT strength and modulus values. For the restrained shrinkage cracking tests, the sides of the beams were sealed and only the top surface was exposed to air to simulate field drying. The shrinkage strain was measured by a linear variable differential transformer (LVDT). IDT strength/modulus tests were conducted after 3, 7, 14, 28, and 56 days of curing.

Coefficient of Thermal Expansion

The COTE is required for determining the thermal strain, which is a key input in the shrinkage cracking model. Figure 3-13 shows the COTE test setup. In this test, a specific temperature cycle was applied, displacements were measured by LVDTs, and temperatures inside the specimens and in the environmental chamber were monitored by thermal couples. The COTE was determined from the cyclic strain, which does not include strain due to autogenous and/or drying shrinkage.

Tests were conducted at different temperature ranges with amplitude set to 9°F and RH maintained constant at either

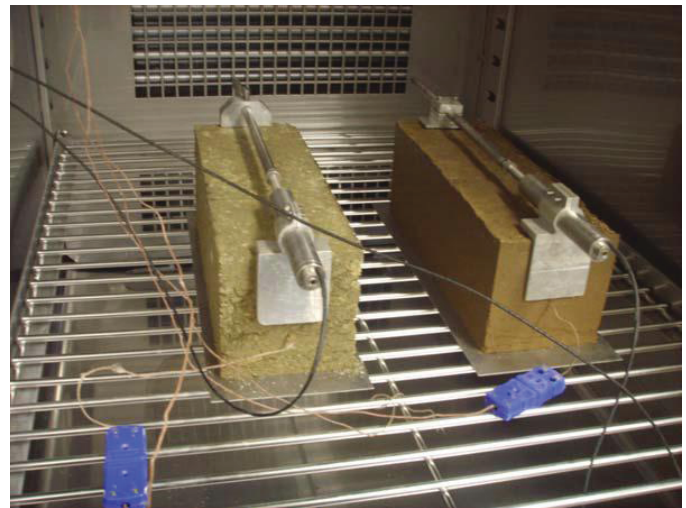


Figure 3-13. COTE test setup (left: gravel–cement; right: clay–lime).

65% or 98%. Figure 3-14 shows the typical change in strain versus time (temperature cycles), and Table 3-8 lists the COTE values for the clay–cement, silt–cement, clay–lime, and gravel–cement at different temperatures and RHs.

Ultimate Drying Shrinkage Strain

Ultimate drying shrinkage strain is the shrinkage strain that develops after extended exposure of CSL to drying conditions. The ultimate drying shrinkage strain was determined from tests on 11.25 × 4 × 4 in. beam specimens stored

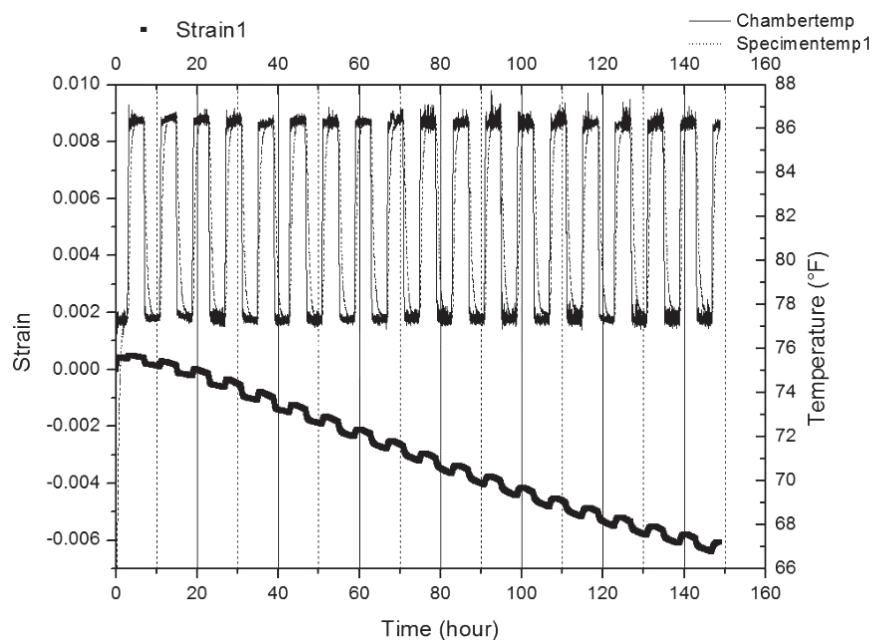


Figure 3-14. Strain versus time for COTE test of clay–lime (77°F to 86°F).

Table 3-8. COTE for different CSM.

Material	Temperature Cycles	Relative Humidity (%)	COTE ($\times 10^{-6}/^{\circ}\text{F}$)
Clay-Cement	68–77°F	65	12.6
Silt-Cement	68–77°F	65	9.3
	104–113°F	65	9.5
Clay-Lime	68–77°F	65	13.1
	77–86°F	98	46.7
	36–45°F	98	29.2
Gravel-Cement	77–86°F	98	14.4
	36–45°F	98	2.6

at 68°F and about 40% RH. The shrinkage strain was measured with dial gauges placed on both sides and monitored until it became stable.

The ultimate drying shrinkage is expressed by the following equation:

$$\epsilon_{su} = C_1 \cdot [w^m + m_2] \tag{3-17}$$

where

ϵ_{su} = ultimate drying shrinkage strain, $\times 10^{-6}$

w = water content, lb/ft³

C_1 = binder type factor: 0.993 for cement, 1.026 for lime, and 0.366 for C fly ash

m_1, m_2 = regression parameters ($m_1 = 3.17, m_2 = 313.76$)

Figure 3-15 shows the measured and predicted ultimate drying shrinkage results.

Drying Shrinkage Strain Gradient

Moisture loss due to evaporation from the top surface of the pavement results in a moisture gradient that leads to self-sustained drying shrinkage stress and early-age cracking in the CSL. The effect of moisture gradient on shrinkage was

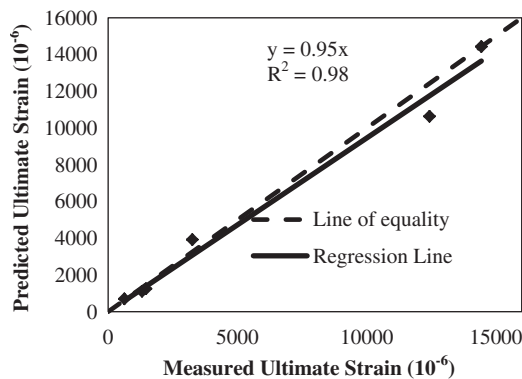


Figure 3-15. Measured versus predicted ultimate drying shrinkage.

investigated in tests on 8 in. tall, 4 in. wide, and 11.25 in. long beams. The four beam sides were sealed with wax leaving only the top surface exposed to air. Figure 3-16 shows the test setup.

The drying shrinkage strain at a specific depth from the surface can be determined from the following equation:

$$\epsilon_g(t) = \epsilon_{su} \left[1 - \left(\frac{RH_c}{100} \right)^{d_6} \right] \tag{3-18}$$

where

$\epsilon_g(t)$ = drying shrinkage strain with moisture gradient at t days from placement, $\times 10^{-6}$

ϵ_{su} = ultimate drying shrinkage strain, $\times 10^{-6}$
(can be estimated from Equation 3-17)

RH_c = calculated relative humidity, %, estimated as follows:

$$RH_c = RH + (100 - RH)f(t)^{d_5}$$

RH = atmospheric relative humidity, %

$$f(t) = 1/(1 + t/b)$$



Figure 3-16. Free-drying shrinkage with moisture gradient test setup.

Table 3-9. Parameters for drying shrinkage strain gradient model.

a_1	a_2	a_3	a_4	a_5	a_6
1289202	0.085	0.94	1.24	10209	4.51

where

t = time since placement in days

$$b = a_1(d + a_2)^{a_3}(w/c)^{a_4}$$

d = depth from evaporation surface, ft

w/c = water/calcium ratio in mass

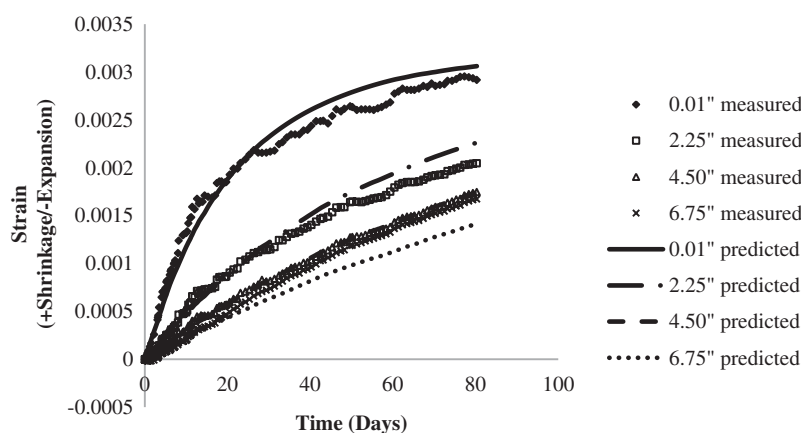
$a_1, a_2, a_3, a_4, a_5, a_6$ = regression parameters (listed in Table 3-9)

Figure 3-17 shows a comparison between the measured and predicted drying shrinkage strain values at various depths for silt–cement and clay–lime maintained at certain temperature and relative humidity.

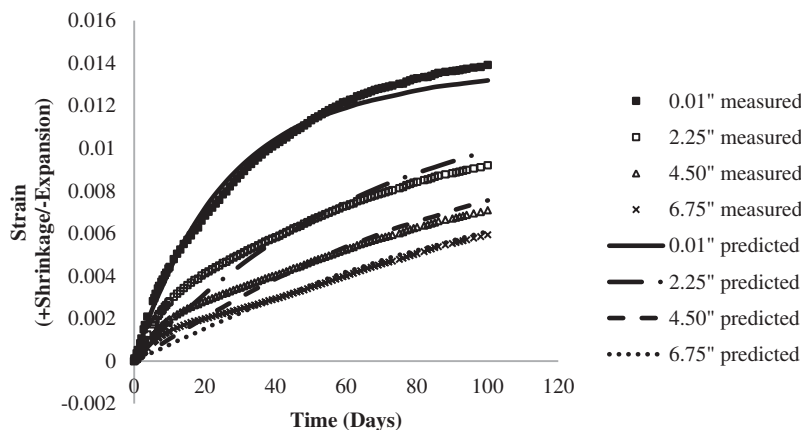
Restrained Shrinkage Cracking

Shrinkage cracking occurs when CSL are restrained by the underlying layer and/or are self-restrained (e.g., by strain gradient). The shrinkage cracking potential of CSL materials can be determined by restrained shrinkage testing. The increase in friction between the CSL and underlying material reduces the shrinkage crack spacing. Shrinkage cracking can be generated in a laboratory specimen by artificially creating a high level of bonding. To simulate the field pavement conditions, the beam sides were sealed, but the surface was exposed to air. The test setup is shown in Figure 3-18.

Clay–cement, clay–lime, and silt–cement beams with dimensions of 48 in. × 6 in. × 4 in. were glued on a steel tube using epoxy. The restrained shrinkage was monitored by an LVDT, and crack spacing and width on the top surface were measured. Figure 3-19 shows typical cracking in the beam specimen and Table 3-10 lists the number of cracks and age when cracking occurred. Actual crack spacing could not be



(a) Silt–Cement at 68°F and 65% RH



(b) Clay–Lime at 68°F and 40% RH

Figure 3-17. Measured versus predicted gradient drying shrinkage strain values at various depths.



Figure 3-18. Restrained shrinkage test setup with sides sealed.

determined from these tests because of the short specimen length and the small number of observed cracks.

Coefficient of Friction

The interface friction/bond affects shrinkage cracking and it is therefore considered in the shrinkage cracking model. For the restrained shrinkage cracking test, the CSM specimen was glued to a steel substrate using epoxy and the coefficient of friction between the CSM and steel substrate was measured using the Iowa shear test (Iowa DOT 2000), which is similar to a direct shear test. In this test, setup shown in Figure 3-20, the load is applied at a constant deformation rate of 0.65 in./min until the CSL is separated from the base layer along the inter-



Figure 3-19. Transverse crack in clay-lime specimen (view from top).

Table 3-10. Laboratory restrained cracking summary.

Materials	Environment	No. of Cracks	Age when Crack Occurred (days)
Clay-Cement	68°F and 65% RH	1	6
	68°F and 40% RH	2	11
	104°F and 40% RH	2	2
Clay-Lime	68°F and 65%RH	1	6
	68°F and 40%RH	1	4
	104°F and 40% RH	1	2
Silt-Cement	68°F and 65% RH	1	10

face, and the coefficient of friction is determined from the slope of the linear portion of the stress-displacement relationship.

When epoxy was used as the bonding agent in the laboratory, the coefficient of friction exhibited a linear relationship with the IDT strength of the CSM, as shown in Figure 3-21. In the field, the CSL bonds well with the underlying layer such that the failure interface usually occurs in the weaker material between the CSM and the underlying material (Romanoschi and Metcalf 2001). Therefore, the slope of the stress versus displacement curve in a direct shear test can be used to estimate the coefficient of friction. Figure 3-22 shows the relationship between the IDT strength of the CSM and the coefficient of friction determined in direct shear tests.

A shrinkage cracking model for predicting crack width and spacing was developed using dimensional analysis, the restrained shrinkage cracking test results, and field data (see Chapter 4).



Figure 3-20. Coefficient of friction test setup.

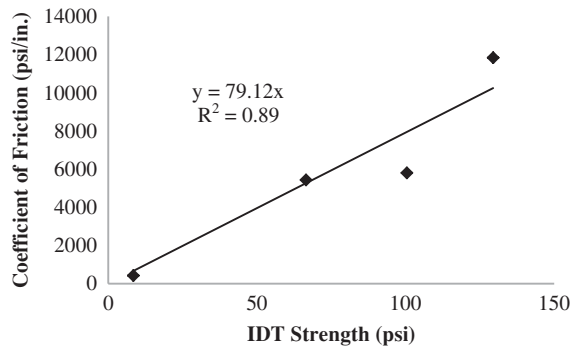


Figure 3-21. IDT strength versus coefficient of friction.

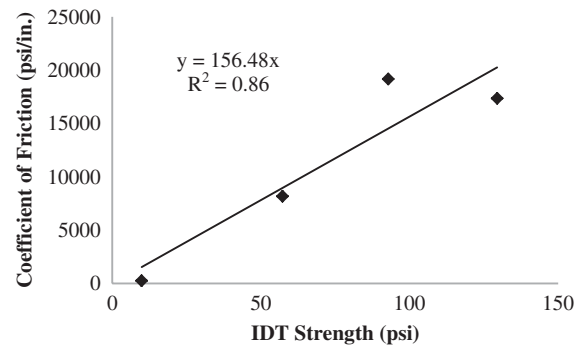


Figure 3-22. IDT strength versus coefficient of friction in a direct shear test.

CHAPTER 4

Model Calibration

Data for Model Calibration

Calibration of the models developed in this study was performed using available field data. However, in those situations where the required data was not available, it was estimated using the relationships developed in this research.

Durability and Fatigue Data

Repeated loads and/or wet–dry and freeze–thaw cycles could damage the CSL located below the pavement surface and result in change in the modulus of the CSL. The modulus value of CSL also increases as a result of continuous hydration and/or pozzolanic reaction. Data were reported in the literature for durability and fatigue tests, including material properties (e.g., 28-day UCS, maximum dry density, and optimum moisture content), field monitoring results [falling weight deflectometer (FWD) modulus values] over time, and traffic information for several locations; these are listed in Table 4-1.

Shrinkage Cracking Data

Information on material properties—such as water content, density, CSL thickness, and UCS—and climatic conditions—such as the actual local daily average temperature and RH—was collected for the sections used for model calibration. Table 4-2 shows a summary of the field data related to CSL shrinkage cracking. Because very limited field data were available, the results from the restrained shrinkage cracking tests were used for calibrating the shrinkage cracking model. The data used for model development were estimated from field data using the procedures described in the following subsections.

Calculation of Crack Spacing and Width

Crack spacing and crack width were reported for some sections but only the total crack length was reported for some

sections. For these cases, it was assumed that only the transverse cracks that extend throughout the entire pavement width existed and there were no longitudinal cracks. The crack spacing is calculated as follows:

$$\text{Crack Spacing} = \frac{\text{section length}}{\frac{\text{total crack length}}{\text{pavement width}}} \quad (4-1a)$$

If the crack spacing is smaller than the pavement width, longitudinal cracking is likely to occur and form a block (square) cracking pattern; the crack spacing is calculated as follows:

$$\text{Crack Spacing} = \frac{\text{section length}}{\frac{\text{total crack length}}{2 \cdot \text{pavement width}}} \quad (4-1b)$$

The crack width is obtained as follows:

$$\text{Crack Width} = \frac{\sum_i^n \text{average crack width of } i\text{th group} \times \text{crack length of } i\text{th group}}{\text{total crack length}} \quad (4-2)$$

where

n = total number of group

For sections with known number of cracks, the average crack spacing is calculated as follows:

$$\text{Crack Spacing} = \frac{\text{section length}}{\text{No. of crack}} \quad (4-3)$$

Coefficient of Friction

The bond between the CSL and underlying material is typically strong, such that bond failure often occurs in the weak

Table 4-1. Sections used for durability and fatigue model calibration.

No.	Source	Section	CSL	FWD Test Location	Traffic at FWD Test Locations
1	Wen et al. (2011)	MnRoad Cell 79 (Minnesota)	Fly ash (14%) + RAP (8 in.)	Mid-Lane	No traffic
2	Bloom Consultants, LLC (2007)	Parking lot in Milwaukee (Wisconsin)	Fly ash (8%) + coal ash (12 in.)	Mid-Lane	No traffic
3		Parking lot ramp in Milwaukee (Wisconsin)	Fly ash (8%) + sandy clay (12 in.)	Mid-Lane	No traffic
4	Bang et al. (2011)	CM1 section, USH 73, Philip (South Dakota)	Cement (3%) + soil (8 in.)	Mid-Lane	No traffic
5		FA1 section, USH 73, Philip (South Dakota)	Fly ash (14%) + soil (8 in.)	Mid-Lane	No traffic
6	Wen et al. (2011)	MnRoad Cell 79 (Minnesota)	Fly ash (14%) + RAP (8 in.)	Mid-Lane	Accelerated
7	Romanoschi et al. (2008)	Indoor, Kansas State University (Kansas)	Cement (7%) + soil (6 in.)	Wheel-Path	Accelerated
8		Indoor, Kansas State University (Kansas)	Fly ash (18%) + soil (6 in.)	Wheel-Path	Accelerated
9		Indoor, Kansas State University (Kansas)	Lime (6%) + soil (6 in.)	Wheel-Path	Accelerated
10	King et al. (1996)	Section 005, Port Allen (Louisiana)	Cement (10%) + soil (8.5 in.)	Wheel-Path	Accelerated
11		Section 006, Port Allen (Louisiana)	Cement (4%) + soil (8.5 in.)	Wheel-Path	Accelerated
12		Section 010, Port Allen (Louisiana)	Cement (4%) + soil (12 in.)	Wheel-Path	Accelerated
13	Bloom Consultants, LLC (2006)	County Highway JK, Waukesha County (Wisconsin)	Fly ash (8%) + RPM (12 in.)	Wheel-Path	ADT 5050, 5% truck
14	Si and Herrera (2007)	Cement kiln dust section, Amarillo District (Texas)	CKD (2%) + local soil (12 in.)	Wheel-Path	ADT 400 (estimated)
15		Fly ash section, Amarillo District (Texas)	Fly ash (8%) + local soil (12 in.)	Wheel-Path	ADT 400 (estimated)
16		Lime section, Amarillo District (Texas)	Lime (3%) + local soil (12 in.)	Wheel-Path	ADT 400 (estimated)
17	Edil et al. (2003)	HW 60, Madison (Wisconsin)	Fly ash (10%) + local soil (12 in.)	Wheel-Path	Design ESAL: 2.6E6

Table 4-2. Summary of CSL data.

Source	Highway	Section	Soil	Binder	Underlying Layer
George (2001)	Highway #302 (Mississippi)	Section 1A	A-2-4	cement (5.5%)	lime (4%) treated subgrade
		Section 3A	A-2-4	cement (5.5%)	lime (4%) treated subgrade
		Section 4	A-2-4	cement (3.5%) and fly ash (8%)	lime (4%) treated subgrade
		Section 6	A-2-4	lime (3%) and fly ash (12%)	lime (4%) treated subgrade
Gaspard (2002)	LA 89 (Louisiana)	Section 1	A-4	cement (9%)	natural silt
		Section 4	A-4	cement (5%)	natural silt
		Section 9	A-4	cement (9%)	natural silt
Sebesta and Scullion (2004), Sebesta (2005)	TAMU Campus (Texas)	4% dry cure	marginal river gravel	cement (4%)	natural gravel
		4% prime cure	marginal river gravel	cement (4%)	natural gravel
		4% moisture cure	marginal river gravel	cement (4%)	natural gravel
		8% dry cure	marginal river gravel	cement (8%)	natural gravel
		8% prime cure	marginal river gravel	cement (8%)	natural gravel
		8% moisture cure	marginal river gravel	cement (8%)	natural gravel
Monlux and Huotari (2012)	Highway #143 (Montana)	Section 2001	A-4	cement (8.7%)	natural silt

Table 4-3. Typical coefficient of friction values (Zhang and Li 2001).

Material in Underlying Layer	Coefficient of Friction (psi/in.)
Cement-Stabilized	13415
Granular	169
Lime-Treated Clay	146
Clay	22

material that lies between the CSL and underlying materials (Romanoschi and Metcalf 2001). Thus, the coefficient of friction for the weak materials between the CSM and underlying material, determined from the direct shear strength test, can be used as Level 1 input. For the Level 2 input, the coefficient of friction can be estimated from the IDT strength, as shown in Figure 3-22. Typical coefficient of friction values for different materials in an underlying layer are listed in Table 4-3 (Zhang and Li 2001); these values are used in this study.

Age of CSL

The age of the CSL is taken as the number of days after construction until shrinkage cracking is observed in the field.

Properties of CSL Materials

Data on density, water content, binder content, and thickness of CSL were obtained from the information reported in the literature. The calcium contents by mass for cement, lime, C fly ash, and F fly ash were assumed to be 63%, 90%, 27%, and 2.7%, respectively (Ramme and Tharaniyil 2004).

The field 28-day UCS values were obtained from data reported in the literature. However, when only the 7-day UCS lab values were provided, the 28-day UCS values were estimated using the growth model given by Equation 3-4. Because no values for the COTE of CSM were available in the literature, COTE values were assumed based on the values used in this study.

Daily Climate Information

Daily climate information, including daily maximum temperature, minimum temperature, and average RH, was obtained from www.wunderground.com/history/.

IDT Strength and Modulus Growth

The cumulative IDT strength/modulus growth was determined using the growth model presented in Equation 3-11.

Ultimate Shrinkage Strain and Shrinkage Strain on Top of CSL

The ultimate shrinkage was determined from Equation 3-17; the cumulative shrinkage strain of the top CSL at any day was estimated from Equation 3-18.

Calibration Procedures

Durability and Fatigue

Calibration of the durability and fatigue model was performed using the following six-step procedure.

Step 1, Determination of Number of Freeze–Thaw and Wet–Dry Cycles in the CSL

The number of freeze–thaw and wet–dry cycles in the CSL was determined based on MEPDG simulations. Input data for the MEPDG were the pavement structure, material properties, and local climate database. The daily frost depth determined by the MEPDG was then used to calculate the freeze–thaw cycles in the CSL. A freeze–thaw cycle consists of freezing of the bottom of the CSL followed by thawing of top of the CSL. The changes in moisture content of the CSL are not considered in the MEPDG although field measurements have shown significant change in CSL moisture (see Figure 4-1). To determine the number of wet–dry cycles, the CSL is substituted by a granular layer in the MEPDG modeling, and the changes in modulus values resulting from the fluctuation of moisture in the unbound materials are determined. The number of modulus cycles in the unbound layers are taken as the number of wet–dry cycles (see Figure 4-2).

Step 2, Prediction of Material Properties for Each Month

Other pavement materials, such as HMA and unbound materials (e.g., subgrade), are also affected by climate. The modulus of HMA is affected by temperature; it varies throughout

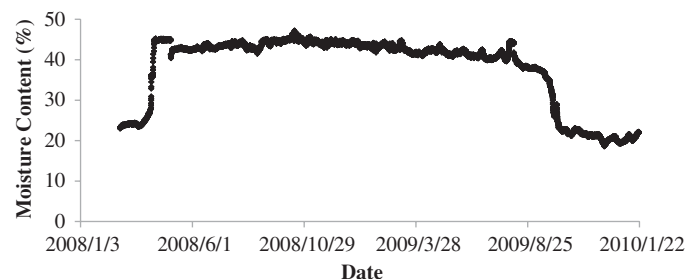


Figure 4-1. Moisture variation in CSL of MnRoad.

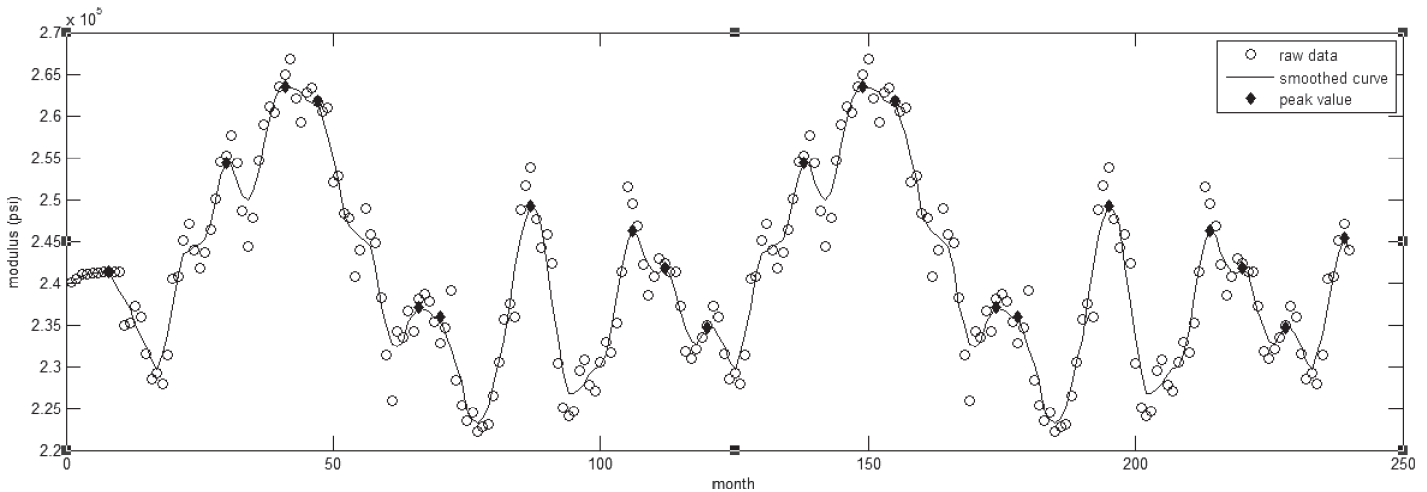


Figure 4-2. Typical wet–dry cycles from MEPDG.

the depth of the HMA layer because of the varying temperature throughout the depth. The modulus of HMA also is affected by oxidation that occurs during pavement life. The modulus of the unbound layer is affected by moisture content and/or temperature (e.g., freezing).

The MEPDG analysis accounts for the effects of climate on HMA and unbound materials. In this analysis, the asphalt layer and unbound material layer are divided into sublayers; the modulus of each sublayer is varied on a monthly basis. The predicted modulus values for the HMA and unbound materials in each sublayer over the course of the pavement life are used in this analysis. The flexural modulus values of the CSL are estimated from the UCS using Equation 3-7. In addition, the modulus values of the CSL are subject to growth and degradation due to the combined effect of wet–dry and freeze–thaw cycles. The growth models and durability models developed in this study were used to determine the combined modulus values of the CSL on a monthly basis.

Step 3, Determination of Pavement Response

After determining the modulus values for the different pavement layers/sublayers, the pavement responses were calculated based on the linear elastic layered theory (Maina and Matsui 2004). The traffic load spectrum, traffic wandering, and temperature distribution were considered using the procedure contained in the MEPDG. Because the modulus growth model and durability models could not be included in the current MEPDG or the Pavement ME Design software, a MATLAB code was developed to calculate the compressive stress on top of the CSL and the tensile stress at the bottom of the CSL on a monthly basis.

Step 4, Determination of Fatigue Life and Damage

After the pavement responses were determined, the bottom-up and top-down fatigue life data were determined using the bottom-up tensile-fatigue and top-down compressive-fatigue–erosion models given by Equations 3-13 and 3-16, respectively. The accumulated damage was then calculated for the applied repetitions of each traffic load level and the corresponding pavement response using Equation 3-14.

Material properties, such as the MOR and the UCS in the top-down compressive-fatigue–erosion model, are also subject to growth and degradation due to wet–dry and freeze–thaw cycles. The strength growth models and durability models were used to determine the change in strength during pavement life on a monthly basis. If the value for the MOR was not readily available, it was determined from the UCS–MOR correlation given by Equation 3-1.

Step 5, Calculation of the Modulus after Damage

The reduction of the modulus of the CSL caused by traffic repetition was estimated from Equation 3-15 for bottom-up tensile-fatigue and top-down compressive-fatigue–erosion damage.

Step 6, Model Calibration

The predicted moduli, after considering growth, durability, and traffic effects, were compared with the FWD backcalculated moduli. The parameters in the fatigue models and damage-modulus model were determined by regression analysis. A flow-chart of the durability and fatigue model calibration process is shown in Figure 4-3.

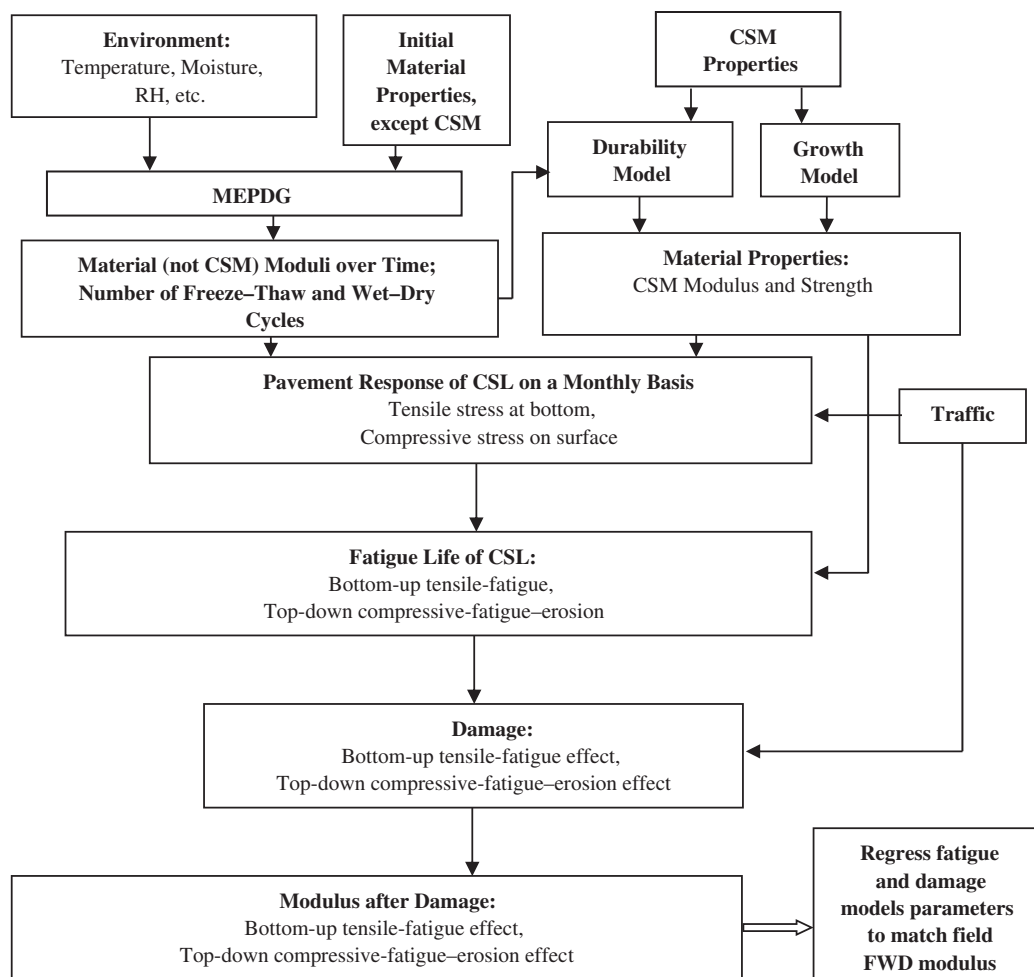


Figure 4-3. Durability and fatigue model calibration process.

Shrinkage Cracking

Different mechanistic models of shrinkage cracking were evaluated but none was deemed appropriate for use in pavement design and analysis (details are provided in Appendix C). Therefore, shrinkage cracking and width models were developed using dimensional analysis and the data collected.

Calibration Results

Durability and Fatigue

FWD Backcalculated Moduli Ratios

A FWD backcalculation evaluation was performed using the deflections of pavements with known layer modulus values (details are provided in Appendix D). The evaluation used the FWD modulus ratio (i.e., the ratio of the modulus of each subsequent FWD measurement to the modulus of the first FWD measurement) to reduce the systematic

error often associated with FWD backcalculation of layer moduli.

Durability Models

Because there was only a limited number of sections for which FWD tests were conducted between the wheel-paths (i.e., with no traffic loading), the durability models developed based on laboratory tests were used. Figure 4-4 presents the predicted modulus ratios versus the backcalculated modulus ratios; the results reflect the error associated with FWD backcalculation (details are provided in Appendix D).

Fatigue Models

The k_2 and k_3 parameters for the bottom-up tensile-fatigue life models (Equation 3-13) were determined from laboratory fatigue tests on different types of materials (Table 3-6). The parameter that accounts for field adjustment, k_1 , and the model

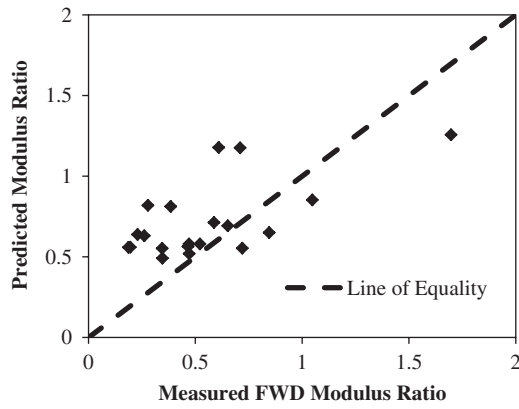


Figure 4-4. Predicted versus backcalculated CSL modulus ratios.

parameters in the modulus-damage models were determined based on field calibrations. Figure 4-5 shows the predicted modulus ratios versus the backcalculated modulus ratios. Table 4-4 lists the model parameters for growth, durability, and fatigue.

Shrinkage Cracking

The shrinkage crack spacing and width models for the CSL were developed based on dimensional analysis (Palmer 2007). Because fine and coarse materials are known to show different shrinkage cracking behaviors (Kodikara and Chakrabarti 2001), model calibrations were carried out for the fine and coarse soil separately; these are presented by Equations 4-4 and 4-5, respectively. Figures 4-6 and 4-7 show the predicted versus measured shrinkage crack spacing in the stabilized fine and coarse layers, respectively. Figures 4-8 and 4-9 show the predicted and measured shrinkage crack widths for the stabilized fine and coarse layers respectively. Tables 4-5 and 4-6 present

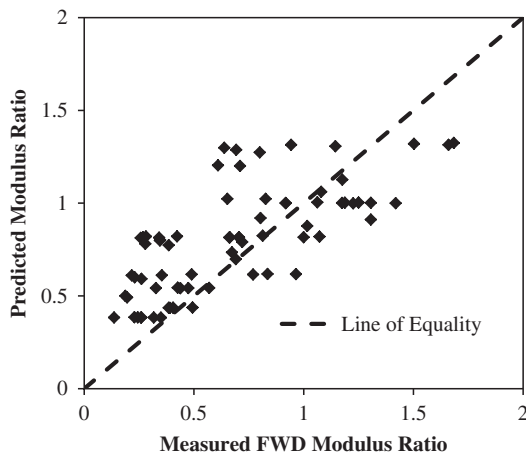


Figure 4-5. Predicted versus measured modulus ratios for fatigue.

Table 4-4. Durability and fatigue model parameters after field calibration.

Model	Equation	Parameter	Value
Growth	3-4	p_1	1.59
		p_2	1.61
Wet-Dry	3-12	m_1	2.58
		n_1	0.62
Freeze-Thaw	3-12	m_1	6.68
		n_1	0.93
Bottom-Up Tensile-Fatigue Life	3-13	k_1	1.07
		k_2	Table 3-6
		k_3	Table 3-6
Top-Down Compressive-Fatigue-Erosion Life	3-16	k_4	10.85
		k_5	1.47
Bottom-Up Tensile-Fatigue Modulus Reduction	3-15	m_2	3.10
		n_2	3.99
Top-Down Compressive-Fatigue-Erosion Modulus Reduction	3-15	m_2	5.08
		n_2	2.01

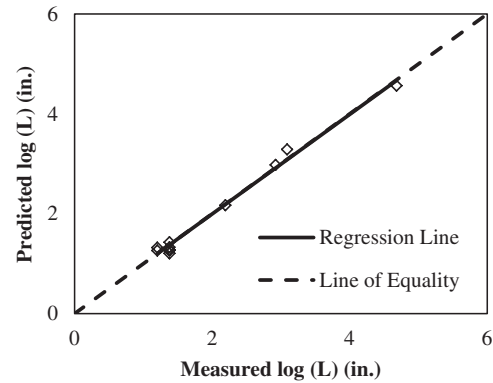


Figure 4-6. Predicted versus measured shrinkage crack spacing for stabilized fine layers.

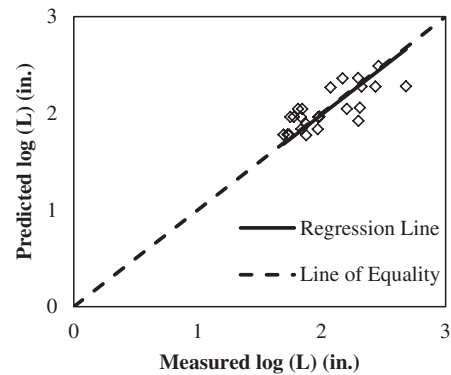


Figure 4-7. Predicted versus measured shrinkage crack spacing for stabilized coarse layers.

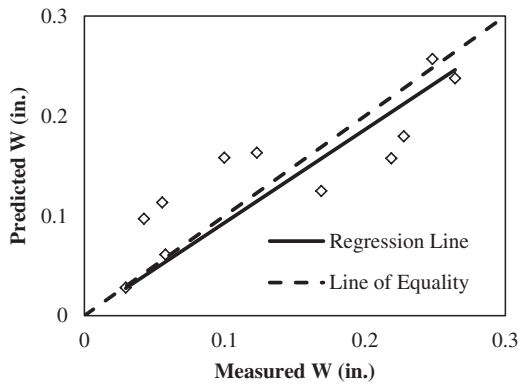


Figure 4-8. Predicted and measured CSL shrinkage crack widths for stabilized fine materials.

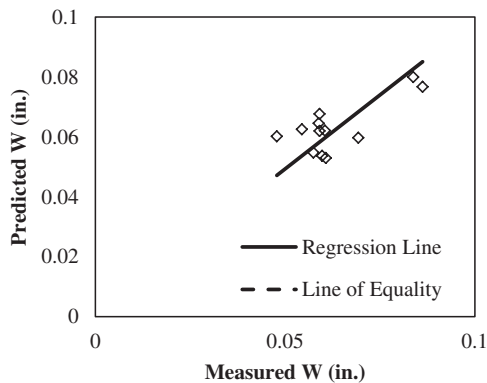


Figure 4-9. Predicted versus measured shrinkage crack widths for stabilized coarse layers.

the model parameters for crack spacing and crack width for stabilized fine and coarse materials, respectively.

$$\log\left(\frac{L}{H}\right) = \left[\begin{array}{l} \left(\frac{\mu}{\rho \cdot H \cdot t^{-2}}\right)^{l_1} \cdot (c\%)^{l_2} \cdot \left(\frac{\omega}{\rho}\right)^{l_3} \\ \cdot (\Delta T \cdot \text{COTE})^{l_4} \cdot \left(\frac{\text{UCS}_{28}}{\rho \cdot H^2 \cdot t^{-2}}\right)^{l_5} \\ \cdot (\text{RH}\%)^{l_6} \cdot \left(\frac{\epsilon_{\text{top}}}{\epsilon_{\text{ult}}}\right)^{l_7} \cdot \left(\frac{\epsilon_{\text{top}} \cdot E_t}{S_{\text{IDT}}}\right)^{l_8} \end{array} \right] \cdot l_9 \quad (4-4)$$

$$W = \left[\begin{array}{l} \left(\frac{\mu}{\rho \cdot H \cdot t^{-2}}\right)^{w_1} \cdot (c\%)^{w_2} \cdot \left(\frac{\omega}{\rho}\right)^{w_3} \\ \cdot (\Delta T \cdot \text{COTE})^{w_4} \cdot \left(\frac{\text{UCS}_{28}}{\rho \cdot H^2 \cdot t^{-2}}\right)^{w_5} \\ \cdot (\text{RH}\%)^{w_6} \cdot \left(\frac{\epsilon_{\text{top}}}{\epsilon_{\text{ult}}}\right)^{w_7} \cdot \left(\frac{\epsilon_{\text{top}} \cdot E_t}{S_{\text{IDT}}}\right)^{w_8} \end{array} \right] \cdot w_9 \quad (4-5)$$

Table 4-5. Parameters for the calibrated CSL shrinkage crack spacing models.

Parameters	Fine Materials	Parameters	Coarse Materials
$l_1 (<0)$	-1.19E-01	$l_1 (<0)$	0
$l_2 (>0)$	5.98E-01	$l_2 (<0)$	-1.39E-01
$l_3 (<0)$	-7.78E-01	$l_3 (<0)$	-1.36E-04
$l_4 (<0)$	0	$l_4 (<0)$	0
$l_5 (>0)$	0	$l_5 (<0)$	-1.46E-01
$l_6 (>0)$	0	$l_6 (>0)$	2.11E+00
$l_7 (<0)$	-2.20E-03	$l_7 (<0)$	0
$l_8 (<0)$	-2.53E-01	$l_8 (<0)$	0
l_9	8.74E+00	l_9	3.85E+00

() contains the parameter constraints.

Table 4-6. Parameters for the calibrated CSL shrinkage crack width models.

Parameters	Fine Materials	Parameters	Coarse Materials
$w_1 (>0)$	7.81E-03	$w_1 (>0)$	0
$w_2 (<0)$	-1.20E+00	$w_2 (>0)$	0
$w_3 (>0)$	7.67E-01	$w_3 (>0)$	1.34E+00
$w_4 (>0)$	0	$w_4 (>0)$	1.76E-05
$w_5 (<0)$	0	$w_5 (>0)$	3.63E-02
$w_6 (<0)$	0	$w_6 (<0)$	0
$w_7 (>0)$	6.69E-01	$w_7 (>0)$	0
$w_8 (>0)$	4.71E-01	$w_8 (>0)$	5.36E-02
w_9	8.63E-04	w_9	1.78E-01

() contains the parameter constraints.

where

L = crack spacing, in.

W = crack width, in.

H = thickness of CSL, in.

μ = coefficient of friction, psi/in., lab from Figure 3-21, field from Table 4-3

ρ = dry density, lb/ft³

t = age when crack survey conducted, days

$c\%$ = calcium content, %

ω = water content, lb/ft³

ΔT = average daily maximum temperature variation, °F

COTE = coefficient of thermal expansion, /°F, from Table 3-8

UCS₂₈ = 28-day UCS at 68°F and 100% RH

RH = average atmosphere relative humidity, %

ϵ_{ult} = ultimate drying shrinkage, calculated by Equation 3-17

ϵ_{top} = shrinkage on the top surface, step-by-step calculated by Equation 3-18 with daily environmental conditions

S_{IDT} = IDT strength, calculated by Equation 3-11a, psi

E_t = IDT modulus, calculated by Equation 3-11b, psi

l_i = regression parameters for crack spacing model, $i = 1, 2, 3, 4, 5, 6, 7, 8,$ and 9

w_i = regression parameters for crack width model, $i = 1, 2, 3, 4, 5, 6, 7, 8,$ and 9

CHAPTER 5

Findings and Recommendations for Research

Findings

The study developed performance models for predicting shrinkage cracking and change of modulus of CSL due to growth, fatigue, freeze–thaw cycles, and wet–dry cycles. Incorporating these models into the MEPDG would allow estimating CSL performance over time on a monthly basis for the prevailing traffic, climate, and materials.

Developed Models and Inputs

The three hierarchical levels adopted in the MEPDG are designated Levels 1, 2, and 3. Level 1 requires site- and/or material-specific inputs obtained through testing or measurements; Level 2 requires inputs estimated from correlations with other information; and Level 3 requires inputs defined by national or regional default values. Growth, durability, fatigue, and shrinkage cracking models developed in this research are listed in Table 5-1. The hierarchical levels of material properties inputs associated with these models are listed in Table 5-2 and are described in the following paragraphs.

Laboratory UCS values after 28-day curing at room temperature and 100% RH were collected from the literature. The range and typical values of the other material properties, including resilient modulus, MOR, flexural modulus, IDT strength, and IDT modulus, were estimated from the UCS values based on the correlations listed in Table 5-2. As noted in Chapter 2, a 7-day UCS of 200 psi was recommended as the criterion for distinguishing between heavily and lightly stabilized materials. This value corresponds to a 28-day UCS of 283 psi based on the strength growth model (Equation 3-4). Therefore, a heavily stabilized material would have a 28-day UCS \geq 283 psi and a lightly stabilized material would have a 28-day UCS $<$ 283 psi. Resilient modulus is recommended for lightly stabilized material only, and flexural modulus for heavily stabilized material only, based on their typical values from literatures and the criteria above.

Equation 5-1 accounts for the growth, durability (wet–dry and freeze–thaw), and fatigue (bottom-up tensile-fatigue and top-down compressive-fatigue–erosion) effects on the strength or modulus.

$$A(t) = A_0 \times \alpha(t) \times \beta(N_{W-D}) \times \lambda(N_{F-T}) \times \gamma(D_{B-T}) \times \eta(D_{T-C}) \quad (5-1)$$

where

$$\begin{aligned} A(t) &= \text{predicted strength or modulus in the field at time } t \\ A_0 &= \text{measured saturated strength or modulus at 28 days} \\ &\quad \text{at 100\% RH curing at } 68^\circ\text{F} \\ t &= \text{time in months} \end{aligned}$$

Effect of Curing Time

$$\alpha(t) = \left[p_1 \left(1 - \frac{1}{1 + \frac{(t-t_0)^2}{p_2}} \right) \right]$$

where

$$\begin{aligned} t_0 &= \text{time in months corresponding to } A_0, \text{ equals to } 28/30.5 \\ p_1, p_2 &= \text{regression parameters, 1.59 and 1.61, respectively,} \\ &\quad \text{as default values} \end{aligned}$$

Effects of Wet–Dry Cycling

$$\beta(N_{W-D}) = \left[\frac{m_1 / \ln(\text{UCS}_{28})}{1 + e^{(mN)}} + 1 - \frac{m_1 / \ln(\text{UCS}_{28})}{2} \right]$$

where

$$\begin{aligned} \text{UCS}_{28} &= \text{28-day UCS, psi} \\ N &= \text{number of wet–dry cycles} \\ m_1, n_1 &= \text{regression parameters for wet–dry durability, 2.58} \\ &\quad \text{and 0.62, respectively, as default values} \end{aligned}$$

Table 5-1. Model description.

Type	Model	Equation	Parameter	Value
Growth	Growth	$S_t = S_{28} \left[p_1 \left(1 - \frac{1}{1 + \frac{(t-t_0)}{p_2}} \right) \right]$	p_1	1.59
			p_2	1.61
Durability	Wet-Dry	$UCS(N) = UCS_{current} \left[\frac{m_1/\ln(UCS_{28})}{1 + e^{(n_1 N)}} + 1 - \frac{m_1/\ln(UCS_{28})}{2} \right]$	m_1	2.58
	Freeze-Thaw	$UCS(N) = UCS_{current} \left[\frac{m_2/\ln(UCS_{28})}{1 + e^{(n_2 N)}} + 1 - \frac{m_2/\ln(UCS_{28})}{2} \right]$	n_1	0.62
Fatigue	Bottom-up Tensile Fatigue	$\ln N_{ft} = k_1 \left(\frac{k_2 - \frac{\sigma_t}{M_{rup}}}{k_3} \right)$	k_1	1.07
			k_2	Table 3-6
			k_3	Table 3-6
	Top-down Compressive Fatigue	$\log N_{fc} = k_4 \left(1 - \frac{\sigma_c}{k_5 UCS} \right)$	k_4	10.85
			k_5	1.47
	Fatigue Damage (Bottom-up and Top-down)	$D = \sum_{i=1}^j \frac{n_i}{N_i}$	n/a	n/a
Bottom-up Tensile-Fatigue Modulus Reduction	$E(D) = E_{current} \left[\frac{m_3/\ln(UCS_{28})}{1 + e^{[\sinh(n_3 D)]}} + 1 - \frac{m_3/\ln(UCS_{28})}{2} \right]$	m_3	3.10	
		n_3	3.99	
Top-down Compressive-Fatigue Modulus Reduction	$E(D) = E_{current} \left[\frac{m_4/\ln(UCS_{28})}{1 + e^{[\sinh(n_4 D)]}} + 1 - \frac{m_4/\ln(UCS_{28})}{2} \right]$	m_4	5.08	
		n_4	2.01	

Type	Model	Equation	Parameter	Fine	Coarse
Shrinkage Crack	Shrinkage Crack Spacing in CSL	$\log\left(\frac{L}{H}\right) = \left[\left(\frac{\mu}{\rho \cdot H \cdot t^{-2}} \right)^{l_1} \cdot (c\%)^{l_2} \cdot \left(\frac{\omega}{\rho} \right)^{l_3} \cdot (\Delta T \cdot COTE)^{l_4} \cdot \left(\frac{UCS_{28}}{\rho \cdot H^2 \cdot t^{-2}} \right)^{l_5} \cdot (RH\%)^{l_6} \cdot \left(\frac{\epsilon_{top}}{\epsilon_{ult}} \right)^{l_7} \cdot \left(\frac{\epsilon_{top} \cdot E_t}{S_{IDT}} \right)^{l_8} \right] \cdot l_9$	l_1	-1.19E-01	0
			l_2	5.98E-01	-1.39E-01
			l_3	-7.78E-01	-1.36E-04
			l_4	0	0
			l_5	0	-1.46E-01
			l_6	0	2.11E+00
			l_7	-2.20E-03	0
			l_8	-2.53E-01	0
			l_9	8.74E+00	3.85E+00
	Shrinkage Crack Width in CSL	$W = \left[\left(\frac{\mu}{\rho \cdot H \cdot t^{-2}} \right)^{w_1} \cdot (c\%)^{w_2} \cdot \left(\frac{\omega}{\rho} \right)^{w_3} \cdot (\Delta T \cdot COTE)^{w_4} \cdot \left(\frac{UCS_{28}}{\rho \cdot H^2 \cdot t^{-2}} \right)^{w_5} \cdot (RH\%)^{w_6} \cdot \left(\frac{\epsilon_{top}}{\epsilon_{ult}} \right)^{w_7} \cdot \left(\frac{\epsilon_{top} \cdot E_t}{S_{IDT}} \right)^{w_8} \right] \cdot w_9$	w_1	7.81E-03	0
			w_2	-1.20E+00	0
			w_3	7.67E-01	1.34E+00
			w_4	0	1.76E-05
			w_5	0	3.63E-02
			w_6	0	0
			w_7	6.69E-01	0
			w_8	4.71E-01	5.36E-02
			w_9	8.63E-04	1.78E-01

Table 5-2. Three levels of input for MEPDG.

Material Properties	Level 1	Level 2	Level 3 (28-day curing at 68°F and 100% RH)	
	Test Procedure	Recommended Relationship	Range	Typical Value
UCS	Test protocol depends on binder and soil type (see notes)	Same to Level 1 input	See Table 5-3	
Resilient Modulus	Mixture design and testing protocol (MDTP) in conjunction with NCHRP 1-28A	$M_r = 0.12 \times \text{UCS} + 9.98$ where M_r = resilient modulus, ksi UCS = unconfined compressive strength, psi	See Table 5-4	
Modulus of Rupture	Proposed test protocol (see Attachment)	$\text{MOR} = 0.14 \times \text{UCS}$ $\text{MOR} = S_{\text{IDT}}/0.86$ where MOR = modulus of rupture, psi UCS = unconfined compressive strength, psi S_{IDT} = IDT strength, psi	See Table 5-5	
Flexural Modulus	Proposed test protocol (see Attachment)	$E_f = 936.28 \times \text{MOR} + 62382$ $E_f = 131.08 \times \text{UCS} + 62382$ where E_f = flexural modulus, psi MOR = modulus of rupture, psi UCS = unconfined compressive strength, psi	See Table 5-6	
IDT Strength	Proposed test protocol (see Attachment)	$S_{\text{IDT}} = 0.12 \times \text{UCS}$ $S_{\text{IDT}} = 0.86 \times \text{MOR}$ where S_{IDT} = IDT strength, psi UCS = unconfined compressive strength, psi. MOR = modulus of rupture, psi	See Table 5-7	
IDT Modulus	Proposed test protocol (see Attachment)	$E_t = 7980.1 \times S_{\text{IDT}}$ $E_t = 957.61 \times \text{UCS}$ where E_t = IDT modulus, psi S_{IDT} = IDT strength, psi UCS = unconfined compressive strength, psi	See Table 5-8	
Coefficient of Thermal Expansion	Proposed test protocol (see Attachment)	Not available	2 to 50 ($10^{-6}/^\circ\text{F}$)	Clay 25.4 ($10^{-6}/^\circ\text{F}$) Silt 9.4 ($10^{-6}/^\circ\text{F}$) Gravel 8.5 ($10^{-6}/^\circ\text{F}$)
Coefficient of Friction	Proposed test protocol (see Attachment)	$\mu = 156.48 \times S_{\text{IDT}}$ where μ = coefficient of friction, psi/in. S_{IDT} = IDT strength, psi	22 to 14000 (psi/in.)	Sublayer type Cement-stabilized, 13415 psi/in. Granular, 169 psi/in. Lime-treated clay, 146 psi/in. Clay, 22 psi/in.

Notes:

 For cement-stabilized fine-grained materials (clay, silt and sand): ASTM D1633, *Standard Test Method for Compressive Strength of Molded Soil-Cement Cylinders*.

 For cement-stabilized granular materials: AASHTO T22, *Standard Method of Test for Compressive Strength of Cylindrical Concrete Specimens*.

 For lime-stabilized clay: ASTM D5102, *Standard Test Method for Unconfined Compressive Strength of Compacted Soil-Lime Mixtures*.

 For fly ash-stabilized soils: ASTM C593, *Standard Specification for Fly Ash and Other Pozzolans for Use with Lime for Soil Stabilization*.

Table 5-3. Level 3 input of UCS (psi).

Binder	Values	Soil				
		Clay	Silt	Sand	Gravel	Recycled Materials
Cement	Range	40 ~ 1015	88 ~ 900	80 ~ 843	392 ~ 1296	30 ~ 1088
	Typical	263	363	350	763	653
Lime	Range	19 ~ 522	78 ~ 510	Not applicable	64 ~ 91	Not applicable
	Typical	150	158	applicable	78	applicable
C fly ash	Range	19 ~ 668	39 ~ 268	31 ~ 693	59 ~ 305	Not applicable
	Typical	181	115	174	214	applicable
Lime and F fly ash	Range	Not applicable	150 ~ 190	Not applicable	Not applicable	120 ~ 200
	Typical	applicable	170	applicable	applicable	190

Table 5-4. Level 3 input of resilient modulus of lightly stabilized materials (ksi).

Binder	Values	Soil				
		Clay	Silt	Sand	Gravel	Recycled Materials
Cement	Range	15 ~ 136	Not applicable	Not applicable	Not applicable	Not applicable
	Typical	43				
Lime	Range	12 ~ 75	20 ~ 73	Not applicable	18 ~ 21	Not applicable
	Typical	29	30		20	
C fly ash	Range	12 ~ 93	15 ~ 43	14 ~ 96	17 ~ 48	Not applicable
	Typical	32	24	32	37	
Lime and F fly ash	Range	Not applicable	29 ~ 34	Not applicable	Not applicable	25 ~ 35
	Typical		31			34

Table 5-5. Level 3 input of modulus of rupture (psi).

Binder	Values	Soil				
		Clay	Silt	Sand	Gravel	Recycled Materials
Cement	Range	6 ~ 142	12 ~ 126	11 ~ 118	55 ~ 181	4 ~ 152
	Typical	37	51	49	107	91
Lime	Range	3 ~ 73	11 ~ 71	Not applicable	9 ~ 13	Not applicable
	Typical	21	25		11	
C fly ash	Range	3 ~ 94	5 ~ 38	4 ~ 97	8 ~ 43	Not applicable
	Typical	25	16	24	30	
Lime and F fly ash	Range	Not applicable	21 ~ 27	Not applicable	Not applicable	17 ~ 28
	Typical		24			27

Table 5-6. Level 3 input of flexural modulus of heavily stabilized materials (ksi).

Binder	Values	Soil				
		Clay	Silt	Sand	Gravel	Recycled Materials
Cement	Range	Not applicable	74 ~ 180	73 ~ 173	114 ~ 232	66 ~ 205
	Typical		110	108	162	148
Lime	Range	Not applicable	Not applicable	Not applicable	Not applicable	Not applicable
	Typical					
C fly ash	Range	Not applicable	Not applicable	Not applicable	Not applicable	Not applicable
	Typical					
Lime and F fly ash	Range	Not applicable	Not applicable	Not applicable	Not applicable	Not applicable
	Typical					

Table 5-7. Level 3 input of IDT strength (psi).

Binder	Values	Soil				
		Clay	Silt	Sand	Gravel	Recycled Materials
Cement	Range	5 ~ 122	11 ~ 108	10 ~ 101	47 ~ 156	4 ~ 131
	Typical	32	44	42	92	78
Lime	Range	2 ~ 63	9 ~ 61	Not applicable	8 ~ 11	Not applicable
	Typical	18	19		9	
C fly ash	Range	2 ~ 80	5 ~ 32	4 ~ 83	7 ~ 37	Not applicable
	Typical	22	14	21	26	
Lime and F fly ash	Range	Not applicable	18 ~ 23	Not applicable	Not applicable	14 ~ 24
	Typical		19			23

Table 5-8. Level 3 input of IDT modulus (ksi).

Binder	Values	Soil				
		Clay	Silt	Sand	Gravel	Recycled Materials
Cement	Range	38 ~ 972	77 ~ 807	77 ~ 807	375 ~ 1241	29 ~ 1042
	Typical	252	335	335	731	625
Lime	Range	18 ~ 500	75 ~ 488	Not applicable	61 ~ 87	Not applicable
	Typical	144	151		74	
C fly ash	Range	18 ~ 640	37 ~ 257	30 ~ 664	57 ~ 292	Not applicable
	Typical	173	110	167	205	
Lime and F fly ash	Range	Not applicable	144 ~ 182	Not applicable	Not applicable	115 ~ 192
	Typical		155			182

Effects of Freeze–Thaw Cycling

$$\lambda(N_{F-T}) = \left[\frac{m_2/\ln(\text{UCS}_{28})}{1 + e^{(m_2 N)}} + 1 - \frac{m_2/\ln(\text{UCS}_{28})}{2} \right]$$

where

UCS₂₈ = 28-day UCS, psi

N = number of freeze–thaw cycles

m₂, n₂ = regression parameters for freeze–thaw durability, 6.68 and 0.93, respectively, as default values

Effects of Bottom-up Tensile Fatigue

$$\gamma(D_{B-T}) = \left[\frac{m_3/\ln(\text{UCS}_{28})}{1 + e^{[\sinh(m_3 D)]}} + 1 - \frac{m_3/\ln(\text{UCS}_{28})}{2} \right]$$

where

D = accumulated damage due to bottom-up tensile fatigue

UCS₂₈ = 28-day UCS, psi

m₃, n₃ = regression parameters for bottom-up tensile-fatigue damage, 3.10 and 3.99, respectively, as default values

Effects of Top-down Compressive Fatigue–Erosion

$$\eta(D_{T-C}) = \left[\frac{m_4/\ln(\text{UCS}_{28})}{1 + e^{[\sinh(m_4 D)]}} + 1 - \frac{m_4/\ln(\text{UCS}_{28})}{2} \right]$$

where

D = accumulated damage due to top-down compressive fatigue–erosion

UCS₂₈ = 28-day UCS, psi

m₄, n₄ = regression parameters for top-down compressive-fatigue–erosion damage, 5.08 and 2.01, respectively, as default values

Quality Control and Quality Assurance

The UCS is used directly in the models or correlated with other material properties in performance models. The 7-day UCS may be used as a QC/QA property. For lightly stabilized materials, such as clay–lime, curing at an accelerated temperature is needed.

Recommendations for Future Research

The following research topics are recommended for consideration:

1. Model validation—The models developed in this research were calibrated based on limited data. Further validation using local field data, especially for the top-down compressive-fatigue–erosion model, would enhance prediction. Because of the errors associated with the FWD backcalculation of CSL, use of field cores of CSM in this validation is encouraged. The modulus of surface layer can be determined from tests on field cores and the modulus of unbound layers can be estimated from the dynamic cone penetrometer.
2. Reflective cracking model—Models are not currently available to predict reflective cracking in asphalt layers placed on CSL. Developing a reflective cracking model that considers shrinkage cracking would enhance performance prediction.
3. Calibration for concrete pavements—Limited data from asphalt pavements were used to calibrate the models developed in this research. Further calibration using data from concrete pavements will enhance validity of these models.
4. Performance-based mix design—CSM mix design is empirical and largely based on trial and error. Developing a performance-based mix design will help better account for traffic levels and local climate.

References

- Applied Research Associates, Inc. 2004. *Guide for Mechanistic–Empirical Design of New and Rehabilitated Pavement Structures* (Final Report, NCHRP Project 1-37A), available at www.trb.org/mepdg
- Atkinson, D. J. 1990. *Evaluation of Rehabilitation Measures for Cracked Cement–Treated Pavements*. Main Road Department 6, Queensland, Australia.
- Austrroads. 2008. *Guide to Pavement Technology: Part 2: Pavement Structural Design*.
- Bang, S. et al. 2011. Quality Base Material Produced Using Full Depth Reclamation on Existing Asphalt Pavement Structure. Final Report No. DTFH61-06-C-00038, Federal Highway Administration.
- Bloom Consultants, LLC. 2006. *Cold In-Place Recycling of Asphalt Pavement with Self-Cementing Fly Ash on County HWY JK in Waukesha County, Wisconsin*. Report for We Energy.
- Bloom Consultants, LLC. 2007. *Stabilization of Class F Coal Ash and Sandy Clay Soil Subgrades for Use of Parking Lot Pavement with Class C Fly Ash in St. Francis, Wisconsin*. Report for We Energy.
- Bonnot, J. 1991. *Semi-rigid Pavements*. Association Internationale Permanente des Congrès de la Route.
- Chen, D. 2007. Field and Lab Investigations of Prematurely Cracking Pavements. *Journal of Performance of Constructed Facilities* (July/August): 293–301.
- Chen, D., P. Harris, T. Scullion, and J. Bilyeu. 2005. Forensic Investigation of a Sulfate-Heaved Project in Texas. *Journal of Performance of Constructed Facilities* (November): 324–330.
- De Beer, M. 1985. Behaviour of Cementitious Subbase Layers in Bitumen Base Road Structures. Masters dissertation, Faculty of Engineering, University of Pretoria, Pretoria.
- De Beer, M. 1990. Aspects of the Design and Behaviour of Road Structures Incorporating Lightly Cementitious Layers. Ph.D. dissertation, Faculty of Engineering, University of Pretoria, Pretoria (February).
- Edil, T. B., C. H. Benson, A. Senol, M. Sazzad Bin-Shafique, B. F. Tanyu, and W. H. Kim. 2003. *Field Performance of Subbases Constructed with Industrial Byproducts and Geosynthetic Reinforcement*. Final Report No. 00-45-18, Wisconsin Department of Transportation.
- Gaspard, K. J. 2002. *In-Place Cement-Stabilized Base Reconstruction Techniques—Interim Report: Construction and Two-Year Evaluation*. LTRC Project No. 95-3GT, Louisiana Transportation Research Center (August).
- George, K. P. 2001. *Soil Stabilization Field Trial—Interim Report*. Interim Report No. FHWA/MS-DOT-RD-03-133, Mississippi Department of Transportation.
- George, K. P. 2002. *Minimizing Cracking in Cement-Treated Materials for Improved Performance*. Portland Cement Association.
- Iowa Department of Transportation. 2000. *Method of Test for Determining Shearing Strength of Bonded Concrete*. Iowa Test 406-C, Ames, IA.
- Jung, Y., D. G. Zollinger, M. Won, and A. J. Wimsatt. 2009. *Subbase and Subgrade Performance Investigation for Concrete Pavement*. Technical Report 6037-1, Texas Transportation Institute.
- King, W. M., K. Gillespie, and G. E. Crosby. 1996. *Construction and Comparison of Louisiana's Conventional and Alternative Base Courses under Accelerated Loading*. Construction Report No. FHWA/LA-97/301, Federal Highway Administration.
- Kodikara, J. and S. Chakrabarti. 2001. *Shrinkage Behaviour of Cemented Materials as Applicable to In Situ Pavement Stabilisation*.
- Li, Y., J. B. Metcalf, S. A. Romanoschi, and M. Rasoulian. 1999. Performance and Failure Modes of Louisiana Asphalt Pavements with Soil–Cement Bases under Full-Scale Accelerated Loading. *Transportation Research Record* 1673: 9–15.
- Little, D. N. and S. Nair. 2007. *Sensitivity of Selected Colorado Soils to Form Ettringite/Thaumasite when Treated with Calcium-Based Stabilizers and when Soluble Sulfates are Available*. Final Report No. CDOT-2007-14, Texas Transportation Institute.
- Luo, R. and J. A. Prozzi. 2008. *Development of Longitudinal Cracks on Pavement over Shrinking Subgrade*. TRB 87th Annual Meeting Compendium of Papers DVD.
- Maina, J. W. and Matsui K. 2004. Developing Software for Elastic Analysis of Pavement Structure Responses to Vertical and Horizontal Surface Loadings. *Transportation Research Record* 1896: 107–118.
- Mallela, J., J. W. Hall, Jr., and K. L. Smith. 2007. Role of Stabilized and Drainable Bases in Early-Age Cracking on Concrete Airfield Pavements. *Transportation Research Record* 2004: 150–162.
- Meng, S., L. Hu, D. Wei, and Y. Li. 2004. The Performance of Stabilized Base Pavements under Accelerated Loading. *Proceedings of the 2004 Accelerated Pavement Testing International Conference*, Minneapolis, MN.
- Metcalf, J. B., F. L. Robert, M. Rasoulian, S. Romanoschi, Y. Li, and L. Djakfar. 2001. *Construction and Comparison of Louisiana's Conventional and Alternative Base Courses under Accelerated Loading*. Final Report Research Project No. 98-3 ALF & Research Project No. 98-2ALF, Louisiana Department of Transportation and Development (November).
- Midgley, L. and R. Yeo. 2008. *The Development and Evaluation of Protocols for the Laboratory Characterisation of Cemented Materials*. Austrroads Publication No. AP–T101/08: 89.
- Monlux, S. and R. Huotari. 2012. Richland County Road Development.

- Naji, K. N. and M. M. Zaman. 2005. Flexural Properties of Stabilized-Aggregate Beams Subjected to Freeze–Thaw Cycles. *TRB 84th Annual Meeting Compendium of Papers CD-ROM*.
- National Lime Association. 2006. Mixture Design and Testing Procedures for Lime Stabilized Soil (October).
- Neal, B. F. and J. H. Woodstrom. 1977. *Faulting of Portland Cement Concrete Pavements*. Report No. FHWA-CA-TL-5167-77-20, California Department of Transportation (July).
- Nussbaum, P. J. and L. D. Childs. 1975. *Repetitive Load Tests of Concrete Slabs on Cement-Treated Subbases*. Portland Cement Association.
- Otte, E. 1978. A Structural Design Procedure for Cement-Treated Layers in Pavements. Ph.D. dissertation, Faculty of Engineering, University of Pretoria.
- Palmer, A. C. 2007. *Dimensional Analysis and Intelligent Experimentation*. World Scientific Publishing Co. Pte Ltd.
- Portland Cement Association. 1992. *Soil–Cement Laboratory Handbook*.
- Pretorius, P. C. and C. L. Monismith. 1972. Fatigue Crack Formation and Propagation in Pavements Containing Soil–Cement Bases. *Highway Research Record* 407: 102–115.
- Ramme, B. and M. Tharaniyil. 2004. *Coal Combustion Products Utilization Handbook*.
- Ramsey, W. J. and O. L. Lund. 1959. *Experimental Lime Stabilization in Nebraska*. Bureau of Public Roads, Hpr-1/6/: 63–104.
- Romanoschi, S. A. and J. B. Metcalf. 2001. Effects of Interface Condition and Horizontal Wheel Loads on the Life of Flexible Pavement Structures. *Transportation Research Record* 1778: 123–131.
- Romanoschi, S., P. Lewis, O. Dumitru, and S. Banda. 2008. *Accelerated Testing for Studying Pavement Design and Performance (FY 2003): Evaluation of the Chemical Stabilized Subgrade Soil (CISL Experiment No. 12)*. Final Report No. FHWA-KS-07-8, Kansas Department of Transportation.
- Ruiz, J. M., R. O. Rasmussen, G. P. Chang, J. C. Dick, and P. K. Nelson. 2005. *Computer-Based Guidelines for Concrete Pavements, Volume II—Design and Construction Guidelines and HIPERPAV II User's Manual*. Final Report No. FHWA-RD-04-121, Office of Infrastructure Research and Development, Federal Highway Administration (February).
- Scullion, T. 2002. *Precracking of Soil–Cement Bases to Reduce Reflection Cracking: Field Investigation*. *Transportation Research Record* 1787: 22–30.
- Scullion, T. and P. Harris. 1998. Forensic Evaluation of Three Failed Cement-Treated Base Pavements. *Transportation Research Record* 1611: 10–18.
- Scullion, T., S. Guthrie, and S. Sebesta. 2003. *Field Performance and Design Recommendations for Full-Depth Recycling in Texas*. Report No. FHWA/TX-03/4182-1, Texas Department of Transportation (March).
- Sebesta, S. and T. Scullion. 2004. *Effectiveness of Minimizing Reflective Cracking in Cement-Treated Bases by Microcracking*. Technical Report No. FHWA/TX-05/0-4502-1, Texas Transportation Institute (October).
- Sebesta, S. 2005. *Continued Evaluation of Microcracking in Texas*. Report No. FHWA/TX-06/0-4502-2, Texas Department of Transportation (November).
- Selezneva, O., J. Jiang, and S. D. Tayabji. 2000. *Preliminary Evaluation and Analysis of LTPP Faulting Data*. Final Report No. FHWA-RD-00-076 (September).
- Sha, A. and L. Hu. 2002. Experimental Study on the Anti-erosion Properties of Pavement Base Materials. *Chinese Journal of Geotechnical Engineering* 24 (3).
- Si, Z. 2008. Forensic Investigation of Pavement Premature Failure due to Soil Sulfate-Induced Heave. *Journal of Geotechnical and Geoenvironmental Engineering* (August): 1201–1204.
- Si, Z. and C. H. Herrera. 2007. Laboratory and Field Evaluation of Base Stabilization Using Cement Kiln Dust. *Transportation Research Record* 1989: 42–49.
- Sobhan, K. and B. M. Das. 2007. Durability of Soil–Cements against Fatigue Fracture. *Journal of Materials in Civil Engineering* 19 (1) (January): 26–32.
- Syed, I., T. Scullion, and R. B. Randolph. 2000. Tube Suction Test for Evaluating Aggregate Base Materials in Frost- and Moisture-Susceptible Environments. *Transportation Research Record* 1709: 78–90.
- Theyse, H. L., M. De Beer, and F. C. Rust. 1996. Overview of South African Mechanistic Pavement Design Method. *Transportation Research Record* 1539: 6–17.
- Thogersen, F. and L. Bjulf. 2005. *Mechanistic Design of Semi-rigid Pavement: An Incremental Approach*. <http://www.vejdirektoratet.dk/publikationer/VIrap138/index.htm>.
- Veisi, M., B. Chittoori, M. Celaya, S. Nazarian, A. J. Puppala, and C. Solis. 2010. *Accelerated Stabilization Design of Subgrade Soils*. Research Report No. TX FHWA/TX 06/0-5569-1 (February).
- Von Quintus, H. L., J. Mallela, and J. Jiang. 2005. Expected Service Life and Performance Characteristics of HMA Pavements in LTPP. *Asphalt Pavement Alliance* (February).
- Wen, H., X. Li, T. Edil, J. O'Donnell, and S. Danda. 2011. *Utilize Cementitious High Carbon Fly Ash (CHCFA) to Stabilize Cold In-place Recycled (CIR) Asphalt Pavement as Base Course*. Phase II Report to the U.S. Department of Energy, Award Number DE-FG02-05EG86238.
- Wise, J. and W. R. Hudson. 1971. *An Examination of Expansive Clay Problem in Texas*.
- Yeo, Y. 2008. Fatigue Performance of Cemented Materials under Accelerated Loading—Influence of Vertical Loading on the Performance of Unbound and Cemented Materials. *Austrroads* (August).
- Zhang, J. and V. Li. 2001. Influence of Supporting Base Characteristics on Shrinkage-Induced Stresses in Concrete Pavements. *Journal of Transportation Engineering* 127 (6) (November/December).
- Zube, E., C. G. Gates, E. C. Shirley, and H. A. Munday. 1969. Service Performance of Cement-Treated Bases as Used in Composite Pavements. *Highway Research Record* 291: 57–69.

ATTACHMENT

Proposed Test Methods

This attachment describes six proposed test methods for measuring properties of CSM:

<u>Page</u>	
34	Modulus of Rupture for Cementitiously Stabilized Materials Using a Simple Beam with Third-Point Loading
39	Flexural Modulus for Cementitiously Stabilized Materials Using Simple Beam with Third-Point Loading
45	Indirect Tensile Strength for Cementitiously Stabilized Materials
50	Indirect Tensile Modulus for Cementitiously Stabilized Materials
58	Coefficient of Thermal Expansion Test of Cementitiously Stabilized Soils
65	Shear Strength Test of Cementitiously Stabilized Soils

These proposed test methods are the suggestions of the NCHRP Project 4-36 research team. These test methods have not been approved by NCHRP or any AASHTO committee nor formally accepted for the AASHTO specifications.

Proposed Standard Method of Test for

Modulus of Rupture for Cementitiously Stabilized Materials Using a Simple Beam with Third-Point Loading

Designation:

1. SCOPE

- 1.1. This test method covers the determination of modulus of rupture of cementitiously stabilized materials by the use of a simple beam specimen subjected to third-point loading. Modulus of rupture, also known as flexural strength, is the material's capability to resist deformation under an applied load.
- 1.2. The values stated in SI units are to be regarded as the standard.
- 1.3. *This standard does not purport to address all of the safety concerns, if any, associated with its use. It is the responsibility of the user of this standard to establish appropriate safety and health practices and determine the applicability of regulatory limitations prior to use.*

2. REFERENCED DOCUMENTS

- 2.1. *AASHTO Standards:*
 - T 22, Standard Method of Test for Compressive Strength of Cylindrical Concrete Specimens
 - T 97, Standard Method of Test for Flexural Strength of Concrete (Using Simple Beam with Third-Point Loading)
 - T 99, Standard Method of Test for Moisture–Density Relations of Soils Using a 2.5 kg Rammer and a 305 mm Drop
 - T 180, Standard Method of Test for Moisture–Density Relations of Soils Using a 4.54 kg Rammer and a 457 mm Drop
- 2.2. *ASTM Standards:*
 - C 593, Standard Specification for Fly Ash and Other Pozzolans for Use with Lime for Soil Stabilization
 - D 558, Standard Test Methods for Moisture–Density (Unit Weight) Relations of Soil–Cement Mixtures
 - D 653, Standard Terminology Relating to Soil, Rock, and Contained Fluids
 - D 1632, Standard Practice for Making and Curing Soil–Cement Compression and Flexure Test Specimens in the Laboratory
 - D 1635, Standard Test Method for Flexural Strength of Soil–Cement Using Simple Beam with Third-Point Loading

3. SUMMARY OF TEST METHOD

- 3.1. Third-point loading tests are conducted on rectangular beam specimens to determine the modulus of rupture of various mixtures. A constant loading is applied until the beam ruptures. After the specimen fails, the peak load and approximate location of the break point are recorded. Testing is conducted under normal laboratory environment conditions at 23°C.

4. SIGNIFICANCE AND USE

- 4.1. This test method is used to determine the modulus of rupture of cementitiously stabilized materials. Modulus of rupture is a key parameter in the analysis of fatigue performance of pavement layers and is used to determine the slab thickness in the pavement design.

5. APPARATUS

- 5.1. *Test Machine*—The testing machine shall conform to the requirements of T 22 and be of a type with sufficient capacity that will provide the rate of loading prescribed in Section 7.5. The apparatus shall be designed to incorporate the following principles:
- 5.1.1. The distance between supports and points of load application shall remain constant for a given apparatus.
- 5.1.2. The load shall be applied at a uniform rate and in such a manner as to avoid shock.
- 5.2. *Loading Apparatus*—The third-point loading method shall be used in conduction flexural tests of cementitiously stabilized material specimens employing bearing blocks, which will ensure that forces applied to the beam will be perpendicular to the face of the specimen and applied without eccentricity. A diagram of an apparatus that accomplishes this purpose is shown in Figure 1. The beam supports are set 300 mm apart to achieve a span to depth ratio of 3. The load positions are at third-points along the sample.

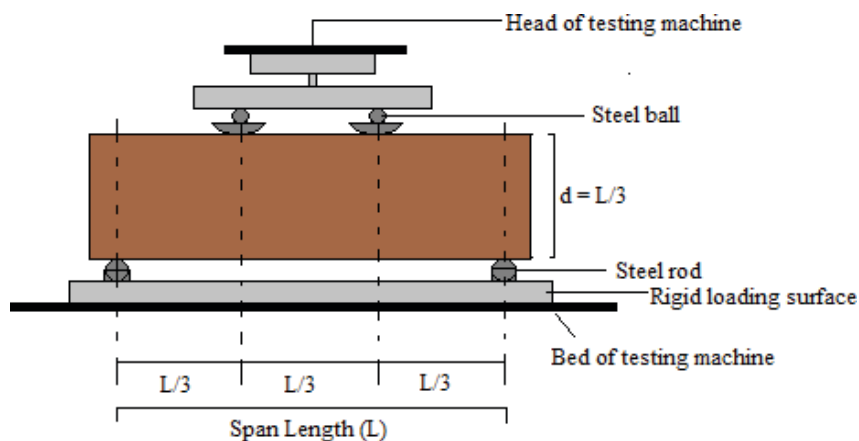


Figure 1— Schematic View of Setup for Flexural Test

- 5.3. *Dial Comparator*—Dial comparator, or other suitable device, for measuring the physical dimensions of the specimen to the nearest 1 mm.

6. TEST SPECIMENS

- 6.1. *Specimen preparation*—Beam specimens are prepared in prismatic molds of dimensions 102×102×400 mm to fabricate the specimens. The moisture content of soil is measured and then the soil is blended with the required percentage by weight of binders until the mixture has uniform color throughout. The soil stabilized (with cement or lime or fly ash) mixture is moistened with water to reach the desired optimum moisture content and blended until uniform; the mixtures are compacted immediately except for lime-stabilized mixture, which should be tightly covered in plastic and allowed to mellow 24 hours before compaction. The specimens are then compacted in three equal layers in the mold to achieve the maximum dry unit weight. The surface between layers is scarified to a depth of 0.6 mm to ensure a good bond. The gravel stabilized specimens are compacted with modified compaction effort (AASHTO T-180); whereas, the sand, silt, and clay stabilized specimens are compacted with standard compaction effort (AASHTO T-99). An appropriate amount of the test material for the specimen is compacted to achieve the target dry unit weight based on the applicable compaction test.
- 6.1.1. Specimens shall be rectangular with smooth, uniform parallel surfaces.
- 6.2. *Core Specimens*—Core undisturbed specimens from large undisturbed samples or from field. Handle specimens carefully to prevent disturbance, changes in cross section, or loss of water content. No moisture curing will be used for core specimens.
- 6.3. *Curing*—Cure the specimens in the molds for 2 days and cover to prevent moisture evaporation at $21\pm 2^{\circ}\text{C}$, and then for a total of 28 days at 100% relative humidity and $21\pm 2^{\circ}\text{C}$.

7. PROCEDURE

- 7.1. *Measurements*—Measure the dimensions of the specimen to the nearest 1 mm; taking at least three measurements for each dimension. Calculate the averages of the three measures for length (l), width (w) and height (h).
- 7.2. Note the span of the apparatus (L).
- 7.3. *Positioning*—Place the beam on the apparatus with respect to its molded position and center it on the lower cylindrical steel supports, which have been spaced. Ensure that the specimen is oriented with the top of the specimen upward.

- 7.4. Modulus of rupture test shall be performed within 30 min of removal from the moisture room/oven.
- 7.5. *Rate of Loading*—A constant load should be applied at a rate of 690 ± 39 kPa/min until the specimen ruptures. Record the maximum applied load indicated by the testing machine at failure. Note the type of failure and the appearance of the specimen.
- 7.6. Three replicates are recommended.

8. CALCULATION

- 8.1. *Calculate the modulus of rupture as follows:*

$$R = PL/bd^2 \quad (1)$$

where:

R = modulus of rupture, kPa;

P = maximum applied load, N;

L = span length, mm;

b = average width of specimen, mm; and

d = average depth of specimen, mm.

9. REPORT

- 9.1. *Report the following information:*
- 9.1.1. Specimen identification number;
- 9.1.2. Average width and depth of the specimen, mm;
- 9.1.3. Span length of the apparatus, mm;
- 9.1.4. Maximum failure load, N;
- 9.1.5. Modulus of rupture calculated from Equation 1, kPa;
- 9.1.6. Age of specimen and curing conditions;
- 9.1.7. Curing history;

- 9.1.8. Defects in specimen;
- 9.1.9. Types of fracture; and
- 9.1.10. Types of specimen.

10. PRECISION AND BIAS

- 10.1. *Precision*—No precision data are available using this test method.
- 10.2. *Bias*—There is no accepted reference value for this test method; therefore, bias cannot be determined.

11. KEYWORDS

- 11.1. Modulus of rupture, flexural strength, cementitiously stabilized materials, soil stabilization

12. REFERENCES

- 12.1. Midgley, L. and R. Yeo. 2008. *The Development and Evaluation of Protocols for the Laboratory Characterisation of Cemented Materials*. Austroads Publication No. AP-T101/08, 89.

Proposed Standard Method of Test for

Flexural Modulus for Cementitiously Stabilized Materials Using Simple Beam with Third-Point Loading

Designation:

1. SCOPE

- 1.1. This test method covers the determination of flexural modulus of cementitiously stabilized materials by the use of a simple beam specimen subjected to third-point loading. Flexural modulus is the measurement of a specified material and cross section to resist bending, when placed under stress.
- 1.2. The values stated in SI units are to be regarded as the standard.
- 1.3. *This standard does not purport to address all of the safety concerns, if any, associated with its use. It is the responsibility of the user of this standard to establish appropriate safety and health practices and determine the applicability of regulatory limitations prior to use.*

2. REFERENCED DOCUMENTS

- 2.1. *AASHTO Standards:*
 - T 99, Standard Method of Test for Moisture–Density Relations of Soils Using a 2.5 kg Rammer and a 305 mm Drop
 - T 180, Standard Method of Test for Moisture–Density Relations of Soils Using a 4.54 kg Rammer and a 457 mm Drop
- 2.2. *ASTM Standards:*
 - C 593, Standard Specification for Fly Ash and Other Pozzolans for Use with Lime for Soil Stabilization
 - D 558, Standard Test Methods for Moisture–Density (Unit Weight) Relations of Soil–Cement Mixtures
 - D 653, Standard Terminology Relating to Soil, Rock, and Contained Fluids
 - D 1632, Standard Practice for Making and Curing Soil–Cement Compression and Flexure Test Specimens in the Laboratory

3. SUMMARY OF TEST METHOD

- 3.1. Third-point loading tests are conducted on rectangular beam specimens to determine the flexural modulus of various mixtures. A dynamic loading is applied for 100 cycles at 1 Hz frequency. During the application of load pulses, the applied peak load and peak displacement of the specimen for each pulse is recorded. Testing is conducted under normal laboratory environment conditions at 23°C.

4. SIGNIFICANCE AND USE

- 4.1. This test method is used to determine the flexural modulus of cementitiously stabilized materials. Flexural modulus is critical for pavement analysis to determine stress/strain and thus, performance prediction. Low modulus of cementitiously stabilized layers (CSL) may lead to high levels of tensile stress at the bottom of the surface layer and, subsequently, bottom tension fatigue cracking.

5. APPARATUS

- 5.1. *Loading Device*—The loading device shall be closed loop, electrohydraulic or electropneumatic testing machine with a function generator that is capable of applying repeated cycles of haversine-shaped load pulse. The apparatus shall be designed to incorporate the following principles:
- 5.1.1. The distance between supports and points of load application shall remain constant for a given apparatus.
- 5.1.2. The load shall be applied at a uniform rate and in such a manner as to avoid shock.
- 5.1.3. The machine shall be capable of applying the load pulse repeatedly until specimen failure.
- 5.2. *Loading Apparatus*—The third-point loading method shall be used in making flexure tests of cementitiously stabilized material specimens employing bearing blocks, which will ensure that forces applied to the beam will be perpendicular to the face of the specimen and applied without eccentricity. A diagram of an apparatus that accomplishes this purpose is shown in Figure 1. The beam supports are set 300 mm apart to achieve a span to depth ratio of 3. The load positions are at third-points along the sample.

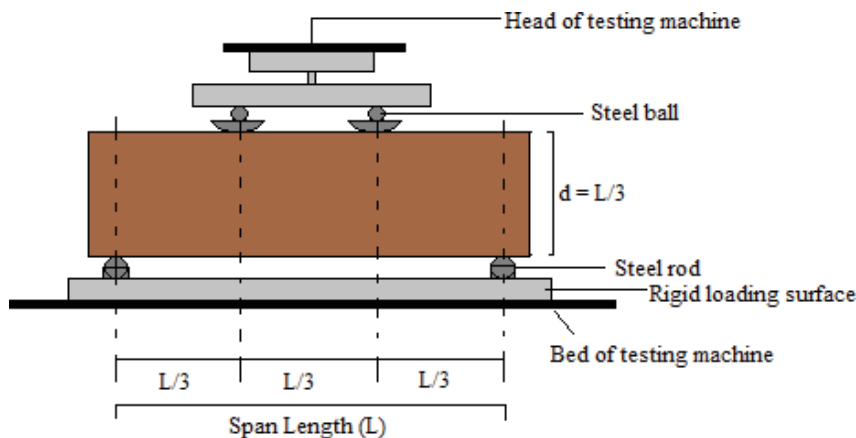


Figure 1—Schematic View of Setup for Flexural Test

- 5.3. *Dial Comparator*—Dial comparator, or other suitable device, for measuring the physical dimensions of the specimen to the nearest 1 mm.
- 5.4. *Displacement-Measuring Device*—Displacement-measuring device for all materials shall consist of two linear variable differential transformers (LVDTs) fixed to opposite sides of the specimen. LVDTs with a range of at least 5 mm, linearity error smaller than $\pm 0.25\%$, and capability of being in contact with the specimen during the complete test are recommended for measurement of horizontal displacement for each pulse.

6. TEST SPECIMENS

- 6.1. *Specimen Preparation*—Beam specimens are prepared in prismatic molds of dimensions 102×102×400 mm to fabricate the specimens. The moisture content of soil is measured and then the soil is blended with the required percentage by weight of binders until the mixture has uniform color throughout. The soil stabilized (with cement or lime or fly ash) mixture is moistened with water to reach the desired optimum moisture content and blended until uniform; the mixtures are compacted immediately except for lime-stabilized mixture, which should be tightly covered in plastic and allowed to mellow 24 hours before compaction. The specimens are then compacted in three equal layers in the mold to achieve the maximum dry unit weight. The surface between layers is scarified to a depth of 0.6 mm to ensure a good bond. The gravel stabilized specimens are compacted with modified compaction effort (AASHTO T-180); whereas, the sand, silt, and clay stabilized specimens are compacted with standard compaction effort (AASHTO T-99). An appropriate amount of the test material for the specimen is compacted to achieve the target dry unit weight based on the applicable compaction test.
- 6.1.1. Specimens shall be rectangular with smooth, uniform parallel surfaces.
- 6.2. *Core Specimens*—Core undisturbed specimens from large undisturbed samples or from field. Handle specimens carefully to prevent disturbance, changes in cross section, or loss of water content. No moisture curing will be used for core specimens.
- 6.3. *Curing*—Cure the specimens in the molds for 2 days and cover to prevent moisture evaporation at $21\pm 2^\circ\text{C}$, and then for a total of 28 days at 100% relative humidity and $21\pm 2^\circ\text{C}$.

7. PROCEDURE

- 7.1. *Measurements*—Measure the dimensions of the specimen to the nearest 1 mm; taking at least three measurements for each dimension. Calculate the averages of the three measures for length (l), width (w) and height (h).
- 7.2. Note the span of the apparatus (L).

- 7.3. *Positioning*—Place the beam on the apparatus with respect to its molded position and center it on the lower cylindrical steel supports, which have been spaced. Ensure that the specimen is oriented with the top of the specimen upwards.
- 7.4. *Displacement Measuring*—The vertical beam displacement is measured using two linear variable differential transformers (LVDTs) at the midpoint of the beam to provide an estimate of the mid-span deflection/strain.
- 7.5. Flexural modulus tests of the specimens are performed within 30 min of removal from the moisture room/oven.
- 7.6. An appropriate peak load (stress level) is determined to apply to the specimen such that the specimen remains within its elastic range. As a guide the fatigue test shall be between 20–40% of the estimated ultimate breaking load (from modulus of rupture tests) of the specimen.
- 7.7. The test is conducted by applying a haversine loading to the specimen for 100 load pulses. The haversine pulse width shall be 250 ms in duration with a 750 ms rest between pulses making a 1000 ms pulse period. A contact load more than 22 N but less than 45 N is applied on the specimen.
- 7.8. Record the maximum force applied to the specimen (P) as indicated by the testing machine, and the peak displacement (δh) for the haversine load pulses applied for each pulse.
- 7.9. Three replicates are recommended.

8. CALCULATION

- 8.1. The first 50 cycles are considered as pre-conditioning. The data from the second 50 consecutive cycles are used to calculate the flexural modulus of the specimen.
- 8.2. *Calculate the flexural modulus as follows:*

$$S_{max} = \frac{23 P L^3}{108 b a^3 \delta h} \times 1000 (I)$$

where:

S_{max} = flexural modulus, MPa;

P = maximum applied load, N;

L = span length, mm;

b = average width of specimen, mm;

d = average depth of specimen, mm; and

δh = peak mid-span displacement, mm.

- 8.3. Average of the second 50 cycles is considered as the flexural modulus of the specimen.

9. REPORT

9.1. *Report the following information:*

9.1.1. Specimen identification number;

9.1.2. Average width and depth of the specimen, mm;

9.1.3. Span length of the apparatus, mm;

9.1.4. Maximum force applied to the specimen, N;

9.1.5. Peak displacement for each load pulse, mm;

9.1.6. Flexural modulus calculated from the average of the second 50 cycles, MPa;

9.1.7. Age of specimen and curing conditions;

9.1.8. Curing history;

9.1.9. Defects in specimen;

9.1.10. Types of fracture; and

9.1.11. Types of specimen.

10. PRECISION AND BIAS

10.1. *Precision*—No precision data are available using this test method.

10.2. *Bias*—There is no accepted reference value for this test method; therefore, bias cannot be determined.

11. KEYWORDS

11.1 Flexural modulus, cementitiously stabilized materials, soil stabilization

12. REFERENCES

- 12.1 Midgley, L. and R. Yeo. 2008. *The Development and Evaluation of Protocols for the Laboratory Characterisation of Cemented Materials*. Austroads Publication No. AP-T101/08, 89.

Proposed Standard Method of Test for

Indirect Tensile Strength for Cementitiously Stabilized Materials

Designation:

1. SCOPE

- 1.1. This test method covers the determination of indirect tensile (IDT) strength of cementitiously stabilized materials.
- 1.2. The values stated in SI units are to be regarded as the standard.
- 1.3. *This standard does not purport to address all of the safety concerns, if any, associated with its use. It is the responsibility of the user of this standard to establish appropriate safety and health practices and determine the applicability of regulatory limitations prior to use.*

2. REFERENCED DOCUMENTS

- 2.1. *AASHTO Standards:*
 - T 22, Standard Method of Test for Compressive Strength of Cylindrical Concrete Specimens
 - T 99, Standard Method of Test for Moisture–Density Relations of Soils Using a 2.5 kg Rammer and a 305 mm Drop
 - T 180, Standard Method of Test for Moisture–Density Relations of Soils Using a 4.54 kg Rammer and a 457 mm Drop
 - T 198, Standard Method of Test for Splitting Tensile Strength of Cylindrical Concrete Specimens
- 2.2. *ASTM Standards:*
 - C 496, Standard Test Method for Splitting Tensile Strength of Cylindrical Concrete Specimens
 - D 6931, Standard Test Method for Indirect Tensile (IDT) Strength of Bituminous Mixtures
 - D 558, Standard Test Methods for Moisture–Density (Unit Weight) Relations of Soil–Cement Mixtures
 - D 653, Standard Terminology Relating to Soil, Rock, and Contained Fluids
 - D 1632, Standard Practice for Making and Curing Soil–Cement Compression and Flexure Test Specimens in the Laboratory

3. SUMMARY OF TEST METHOD

- 3.1. This test method consists of applying a diametral compressive force along the length of a cylindrical specimen at a rate that is within a prescribed range until failure

occurs. This loading induces tensile stresses on the plane containing the applied load and relatively high compressive stresses in the area immediately around the applied load. Tensile failure occurs rather than compressive failure.

- 3.2. Aluminum bearing blocks are used to distribute the load applied along the length of the cylinder.
- 3.3. The maximum load sustained by the specimen is divided by appropriate geometrical factors to obtain the splitting tensile strength.

4. SIGNIFICANCE AND USE

- 4.1. This test method is used to determine the IDT strength of cementitiously stabilized materials. IDT strength is a key parameter in the analysis of shrinkage cracking of cementitiously stabilized layers.

5. APPARATUS

- 5.1. *Testing Machine*—The testing machine shall conform to the requirements of T 22 and be of a type with sufficient capacity that will provide the rate of loading prescribed in Section 7.4.
- 5.2. *Plano-Cylindrical-Concave Bearing Blocks*—Two bearing blocks, free of imperfections, of a length equal to, or slightly longer than, that of the specimen shall be provided for each specimen. The loading surface on the bearing blocks shall be flat, and the surface in contact with the specimen shall be concave. The distance between the curved and flat surfaces shall not be less than 18 mm at the thinnest section. Table 1 shows the width of the bearing blocks as measured from tip to tip of the concave face, and the radius of the curvature.

Table 1—Width and Radius of Curvature of Bearing Blocks (mm)

Nominal diameter of specimen	Width of bearing blocks	Radius of curvature of the concave face
152.4	19.05 ± 2.0	75 ± 2.0

- 5.3. *Dial Comparator*—Dial comparator, or other suitable device, for measuring the physical dimensions of the specimen to the nearest 0.1 mm (Note 1).

Note 1—Vernier calipers are not recommended for soft specimens, which will deform as the calipers are set on the specimen.

6. TEST SPECIMENS

- 6.1. *Specimen Preparation*—Cylindrical specimens are prepared in cylinder molds. The moisture content of soil is measured and then the soil is blended with the required percentage by weight of binders until the mixture has uniform color throughout. The soil stabilized (with cement or lime or fly ash) mixture is moistened with water to reach the desired optimum moisture content and blended until uniform; the mixtures are compacted immediately. The specimens are then compacted in one layer in the mold to achieve the maximum dry unit weight. The gravel stabilized specimens are compacted with modified compaction effort (AASHTO T-180); whereas, the sand, silt, and clay stabilized specimens are compacted with standard compaction effort (AASHTO T 99). An appropriate amount of the test material for the specimen is compacted to achieve the target dry unit weight based on the applicable compaction test. Specimens shall have smooth, uniform parallel surfaces.
- 6.2. *Core Specimens*—Core undisturbed specimens from large undisturbed samples or from field. Handle specimens carefully to prevent disturbance, changes in cross section, or loss of water content. No moisture curing will be used for core specimens.
- 6.3. *Curing*—Cure the specimens for a total of 28 days at 100% relative humidity and $21 \pm 2^\circ\text{C}$.
- 6.4. *Test specimens*—The nominal dimensions of the cylindrical samples should be 152.4 mm in diameter by 60 to 85 mm in height.

7. PROCEDURE

- 7.1. *Marking*—Draw diametral lines on each end of the specimen using a suitable device that will ensure that they are in the same axial plane.
- 7.2. *Measurements*—Determine the diameter of the test specimen to the nearest 0.1 mm by averaging three diameters measured near the ends and the middle of the specimen and lying in the plane containing the lines marked on the two ends. Determine the length of the specimen to the nearest 0.1 mm by averaging at least two length measurements taken in the plane containing the lines marked on the two ends.
- 7.3. *Positioning Using Marked Diametral Lines*—Place the specimen on the lower bearing block and align so that the lines marked on the ends of the specimen are vertical and horizontal, and centered over the bearing block. Place a second bearing block lengthwise on the cylinder, centered on the lines marked on the ends of the cylinder.
- 7.4. *Rate of Loading*—Apply the load continuously and without shock, at a constant rate of 100 ± 5 kPa/min splitting tensile stress or at a constant rate of displacement corresponding to this splitting tensile stress, until failure of the specimen (Note 2).

Record the maximum applied load indicated by the testing machine at failure. Note the type of failure and the appearance of the specimen.

Note 2—The relationship between splitting tensile stress and applied load is shown in Section 8.

- 7.5. Three replicates are recommended.

8. CALCULATION

- 8.1. Calculate the splitting strength of the specimen as follows:

$$S_t = \frac{2P}{\pi ld} (I)$$

where:

S_t = IDT strength, Pa

P = maximum applied load indicated by the testing machine, N

l = height of the specimen, m

d = diameter of the specimen, m

9. REPORT

- 9.1. Report the following information:
- 9.1.1. Specimen identification number;
 - 9.1.2. Average diameter and length of the specimen, m;
 - 9.1.3. Maximum failure load, N;
 - 9.1.4. IDT strength calculated from Equation 1, Pa;
 - 9.1.5. Age of specimen and curing conditions;
 - 9.1.6. Curing history;
 - 9.1.7. Defects in specimen;
 - 9.1.8. Types of fracture; and
 - 9.1.9. Types of specimen.

10. PRECISION AND BIAS

- 10.1. *Precision*—No precision data are available using this test method.
- 10.2. *Bias*—There is no accepted reference value for this test method; therefore, bias cannot be determined.

11. KEYWORDS

- 11.1 Indirect tensile (IDT) strength; splitting tension; cementitiously stabilized materials; soil stabilization.

12. REFERENCES

- 12.1. Midgley, L. and R. Yeo. 2008. *The Development and Evaluation of Protocols for the Laboratory Characterisation of Cemented Materials*. Austroads Publication No. AP-T101/08, 89.

Proposed Standard Method of Test for

Indirect Tensile Modulus for Cementitiously Stabilized Materials

Designation:

1. SCOPE

- 1.1. This test method covers the determination of indirect tensile (IDT) modulus of cementitiously stabilized materials.
- 1.2. The values stated in SI units are to be regarded as the standard.
- 1.3. *This standard does not purport to address all of the safety concerns, if any, associated with its use. It is the responsibility of the user of this standard to establish appropriate safety and health practices and determine the applicability of regulatory limitations prior to use.*

2. REFERENCED DOCUMENTS

- 2.1. *AASHTO Standards:*
 - T 99, Standard Method of Test for Moisture–Density Relations of Soils Using a 2.5 kg Rammer and a 305 mm Drop
 - T 180, Standard Method of Test for Moisture–Density Relations of Soils Using a 4.54 kg Rammer and a 457 mm Drop
 - T307, Standard Method of Test for Determining the Resilient Modulus of Soils and Aggregate Materials
- 2.2. *ASTM Standards:*
 - C 496, Standard Test Method for Splitting Tensile Strength of Cylindrical Concrete Specimens
 - D 6931, Standard Test Method for Indirect Tensile (IDT) Strength of Bituminous Mixtures
 - D 558, Standard Test Methods for Moisture–Density (Unit Weight) Relations of Soil–Cement Mixtures
 - D 653, Standard Terminology Relating to Soil, Rock, and Contained Fluids
 - D 1632, Standard Practice for Making and Curing Soil–Cement Compression and Flexure Test Specimens in the Laboratory

3. SUMMARY OF TEST METHOD

- 3.1. This test method consists of laboratory determination of the resilient modulus of cementitiously stabilized materials using cyclic load in indirect tensile test mode. The IDT modulus is the ratio of the amplitude of the repeated tensile stress to the

amplitude of the resultant resilient horizontal strain on the plane containing the applied load.

- 3.2. Aluminum bearing blocks are used to distribute the load applied along the length of the cylinder.
- 3.3. Resilient horizontal strain is defined as the difference between the peak horizontal strain associated with a load pulse and the horizontal strain at the end of the rest time of the load pulse.

4. SIGNIFICANCE AND USE

- 4.1. This test method is used to determine the IDT modulus of cementitiously stabilized materials. IDT modulus is a key parameter in the analysis of shrinkage cracking of cementitiously stabilized layers.

5. APPARATUS

- 5.1. *Loading Device*—The loading device shall be a closed loop, electrohydraulic or electropneumatic testing machine with a function generator that is capable of applying repeated cycles of haversine-shaped load pulse.
- 5.2. *Load-Measuring Device*—The axial load-measuring device should be an electronic load cell located between the actuator and the bearing block and have capacity equal to or greater than the maximum capacity of the loading ram.
- 5.3. *Displacement-Measuring Device*—Displacement-measuring device for all materials shall consist of two linear variable differential transformers (LVDTs) fixed to opposite sides of the specimen. LVDTs with a range of at least 5 mm, linearity error smaller than $\pm 0.25\%$, and capability of being in contact with the specimen during the complete test are recommended for measurement of horizontal displacement for each pulse.
- 5.4. *Plano-Cylindrical-Concave Bearing Blocks*—Two bearing blocks, free of imperfections, of a length equal to, or slightly longer than, that of the specimen shall be provided for each specimen. The loading surface on the bearing blocks shall be flat, and the surface in contact with the specimen shall be concave. The distance between the curved and flat surfaces shall not be less than 18 mm at the thinnest section. Table 1 shows the width of the bearing blocks as measured from tip to tip of the concave face, and the radius of the curvature.

Table 1—Width and Radius of Curvature of Bearing Blocks (mm)

Nominal diameter of specimen	Width of bearing blocks	Radius of curvature of the concave face
152.4	19.0 ± 2.0	75 ± 2.0

- 5.5. *Dial Comparator*—Dial comparator, or other suitable device, for measuring the physical dimensions of the specimen to the nearest 0.1 mm (Note 1).

Note 1—Vernier calipers are not recommended for soft specimens, which will deform as the calipers are set on the specimen.

6. TEST SPECIMENS

- 6.1. *Specimen Preparation*—Cylindrical specimens are prepared in cylinder molds. The moisture content of soil is measured and then the soil is blended with the required percentage by weight of binders until the mixture has uniform color throughout. The soil stabilized (with cement or lime or fly ash) mixture is moistened with water to reach the desired optimum moisture content and blended until uniform; the mixtures are compacted immediately. The specimens are then compacted in one layer in the mold to achieve the maximum dry unit weight. The gravel stabilized specimens are compacted with modified compaction effort (AASHTO T-180); whereas, the sand, silt, and clay stabilized specimens are compacted with standard compaction effort (AASHTO T 99). An appropriate amount of the test material for the specimen is compacted to achieve the target dry unit weight based on the applicable compaction test. Specimens shall have smooth, uniform parallel surfaces.
- 6.2. *Core Specimens*—Core undisturbed specimens from large undisturbed samples or from field. Handle specimens carefully to prevent disturbance, changes in cross section, or loss of water content. No moisture curing will be used for core specimens.
- 6.3. *Curing*—Cure the specimens for a total of 28 days at 100% relative humidity and $21 \pm 2^\circ\text{C}$.
- 6.4. *Test Specimens*—The nominal dimensions of the cylindrical samples should be 152.4 mm in diameter by 60 to 85 mm in height.

7. PROCEDURE

- 7.1. *Marking*—Draw diametral lines on each end of the specimen using a suitable device that will ensure that they are in the same axial plane.
- 7.2. *Measurements*—Determine the diameter of the test specimen to the nearest 0.1 mm by averaging three diameters measured near the ends and the middle of the specimen and lying in the plane containing the lines marked on the two ends. Determine the length of the specimen to the nearest 0.1 mm by averaging at least two length measurements taken in the plane containing the lines marked on the two ends.
- 7.3. *Positioning the LVDTs*—Place LVDTs on the specimen along the horizontal diametric marking to measure the horizontal deformation. The gauge length should be 101.6 mm for 152.4 mm diameter specimen, as shown in Figure 1.

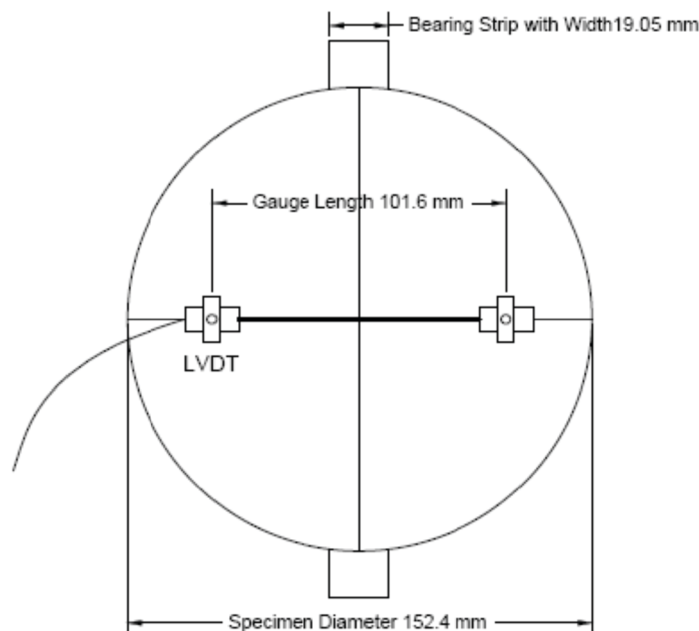
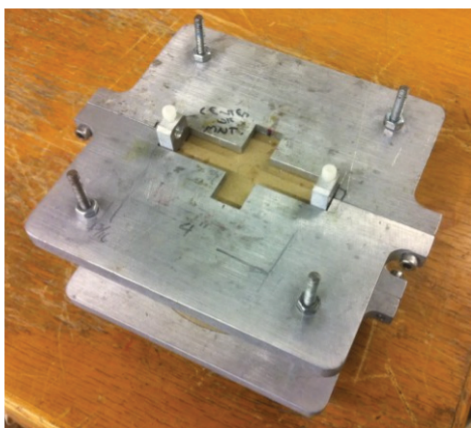


Figure 1—IDT Modulus Test Setup

- 7.3.1. For granular material, position the specimen using a suitable device that will ensure that they are stable, such as that shown in Figure 2. Glue the LVDT mounts with quick-setting epoxy on one side first. After the epoxy is set, flip over the specimen, and glue the LVDT mounts on the other side.



Outside of the Aligning Jig



Inside of the Aligning Jig

Figure 2—Aligning Jig for Gluing LVDT Mounts on the Specimen

- 7.3.2. For fine materials, drill holes on both sides of the specimen with diameter equal to or smaller than the diameter of the screws (pan-head Phillips screw for sheet metal 18-8 stainless steel, No. 2 size, 3/8 in. length). Fasten each LVDT mount with two holes along the marked diametral lines. Use aligning jig, as shown in Figure 3, to make sure all four holes are aligned along the diametral line. After drilling all the holes on both sides, fasten the LVDT mounts with No. 2 screws.



Drill Press and Specimen

Top View of the Aligning Jig.

Figure 3—Drill Press and Aligning Jig for Fastening LVDT Mounts with Screws

- 7.4. *Positioning Using Marked Diametral Lines*—Place the specimen on the lower bearing block and align so that the lines marked on the ends of the specimen are vertical and horizontal, and centered over the bearing block. Place a second bearing block lengthwise on the cylinder, centered on the lines marked on the ends of the cylinder.
- 7.5. *Indirect Tensile Strength*—Prior to the commencement of the modulus test the indirect tensile strength shall be determined on a separate set of specimens using the draft Standard Method of Test for Indirect Tensile Strength for Cementitiously Stabilized Materials.
- 7.6. *Indirect Tensile Modulus*—To determine the specimen IDT modulus, apply peak load such that the material response remains within its elastic range. Thirty percent of IDT strength is recommended as a typical load level. Apply a contact load, which is about 44 N, to the specimen before the test. Apply 100 repetitions of the corresponding cyclic axial stress using a haversine-shaped load pulse with a 0.1 s duration followed by a rest period of 0.9 s duration.
- 7.7. Three replicates are recommended.

8. CALCULATION

8.1. The first 90 cycles are considered as pre-conditioning. The data from the last 10 cycles are used to calculate the IDT modulus of the specimen.

8.2. Calculate the IDT resilient modulus as follows:

$$\sigma = \frac{2P}{\pi ld} \quad (1)$$

$$\varepsilon = U \frac{\gamma_1 + \gamma_2 \nu}{\gamma_3 + \gamma_4 \nu} \quad (2)$$

$$E_{IDT} = \frac{\sigma}{\varepsilon} \quad (3)$$

where:

σ = tensile stress, Pa

P = maximum applied load indicated by the testing machine, N

l = height of the specimen, m

d = diameter of the specimen, m

U = horizontal displacement, m

ν = Poisson's ratio, 0.2 for cementitiously stabilized material

E_{IDT} = indirect tensile modulus, Pa

$\gamma_1, \gamma_2, \gamma_3, \gamma_4$ = parameters dependent on diameter of specimen, gauge length, and bearing block width, which can be found in Tables 2 and 3 for bearing block width of 19.05 and 12.7 mm, respectively. The details on derivation and calculation of the parameters may be found elsewhere (Hondros 1959; and Kim et al 2001).

Table 2—Parameters when Bearing Block Width is 19.05 mm

Diameter (mm)	Gauge Length (mm)	γ_1	γ_2	γ_3	γ_4
101.6	25.4	17.97	55.70	0.4226	1.3431
	50.8	17.97	55.70	0.6873	2.3294
	76.2	17.97	55.70	0.7829	2.8494
152.4	25.4	12.27	37.34	0.3007	0.9259
	50.8	12.27	37.34	0.5434	1.7290
	76.2	12.27	37.34	0.7000	2.3342
	101.6	12.27	37.34	0.7781	2.7269
	127.0	12.27	37.34	0.8043	2.9328

Table 3—Parameters when Bearing Block Width is 12.7 mm

Diameter (mm)	Gauge Length (mm)	γ_1	γ_2	γ_3	γ_4
101.6	25.4	12.27	37.34	0.2880	0.8993
	50.8	12.27	37.34	0.4667	1.5561
	76.2	12.27	37.34	0.5305	1.9005
152.4	25.4	8.27	24.95	0.2025	0.6186
	50.8	8.27	24.95	0.3655	1.1545
	76.2	8.27	24.95	0.4704	1.5575
	101.6	8.27	24.95	0.5225	1.8186
	127.0	8.27	24.95	0.5399	1.9554

9. REPORT

9.1. *Report the following information:*

- 9.1.1. Specimen identification number;
- 9.1.2. Average diameter and length, m;
- 9.1.3. Load level in IDT modulus test;
- 9.1.4. IDT modulus calculated from Equations 1 to 3, Pa;
- 9.1.5. Age of specimen and curing conditions;
- 9.1.6. Curing history;
- 9.1.7. Defects in specimen;
- 9.1.8. Types of fracture; and
- 9.1.9. Types of specimen.

10. PRECISION AND BIAS

- 10.1. *Precision*—No precision data are available using this test method.
- 10.2. *Bias*—There is no accepted reference value for this test method; therefore, bias cannot be determined.

11. KEYWORDS

- 11.1 Indirect tensile (IDT) modulus, cementitiously stabilized materials, soil stabilization

12. REFERENCES

- 12.1. Midgley, L. and R. Yeo. 2008. *The Development and Evaluation of Protocols for the Laboratory Characterisation of Cemented Materials*. Austroads Publication No. AP-T101/08, 89.
- 12.2. Hondros G. 1959. Evaluation of Poisson's Ratio and Modulus of Materials of a Low Tensile Resistance by Brazilian (Indirect Tensile) Test with Particular Reference to Concrete. *Australian Journal of Applied Science*, 10(3): 243–268.
- 12.3. Kim, Y. R., J. S. Daniel, and H. Wen. 2001. *Fatigue Performance Evaluation of WesTrack Mixtures Using Direct Tension and Indirect Tension Tests*. Final Report submitted to North Carolina Department of Transportation and FWHA.

Proposed Standard Method of Test for

Coefficient of Thermal Expansion Test of Cementitiously Stabilized Soils

Designation:

1. SCOPE

- 1.1. This test method covers determination of the coefficient of thermal expansion (COTE) of cementitiously stabilized soil at early age due to temperature variation other than externally applied forces.
- 1.2. The values stated in SI units are to be regarded as the standard. The English unit equivalents shown in parentheses may be appropriate, except with regard to sieve sizes and aggregate size as determined by the use of testing sieves, in which case the standard SI designation shown is the standard as required by AASHTO Specification M 92.
- 1.3. *This standard may involve hazardous materials, operations, and equipment. This standard does not purport to address all of the safety problems associated with its use. It is the responsibility of the user of this standard to establish appropriate safety and health practices and determine the applicability of regulatory limitations prior to use.*

2. REFERENCED DOCUMENTS

- 2.1. *AASHTO Standards:*
 - M 92, Wire-Cloth Sieves for Testing Purposes
 - M 210, Use of Apparatus for the Determination of Length Change of Hardened Cement Paste, Mortar, and Concrete
 - T 180, Moisture–Density Relations of Soils Using a 4.54 kg (10 lb) Rammer and a 457 mm (18 in.) Drop
- 2.2. *ASTM Standards:*
 - D 698, Standard Test Methods for Laboratory Compaction Characteristics of Soil Using Standard Effort

3. SUMMARY OF TEST METHOD

- 3.1. This test method consists of applying temperature cycles at a constant relative humidity condition on a cementitiously stabilized prism specimen and measuring the deformation due to temperature cycling.

- 3.2. The amplitude of strain cycles during the temperature cycles of the specimen is divided by the amplitude of temperature cycle to determine the COTE value.

4. SIGNIFICANCE AND USE

- 4.1. This test method is used to determine the COTE value of cementitiously stabilized materials. COTE is critical for thermal shrinkage strain and is a key parameter in the analysis of shrinkage cracking of cementitiously stabilized layers.

5. APPARATUS

- 5.1. *Molds*—The molds for casting test specimens shall conform to the requirements of M 210 with internal dimension 101.6 mm × 101.6 mm × 285.75 mm (4 in. × 4 in. × 11.25 in.). A 50.8 mm (2 in.) tall extension collar should be fixed on the mold with screws. The extension collar shall be constructed as shown in Figure 1.

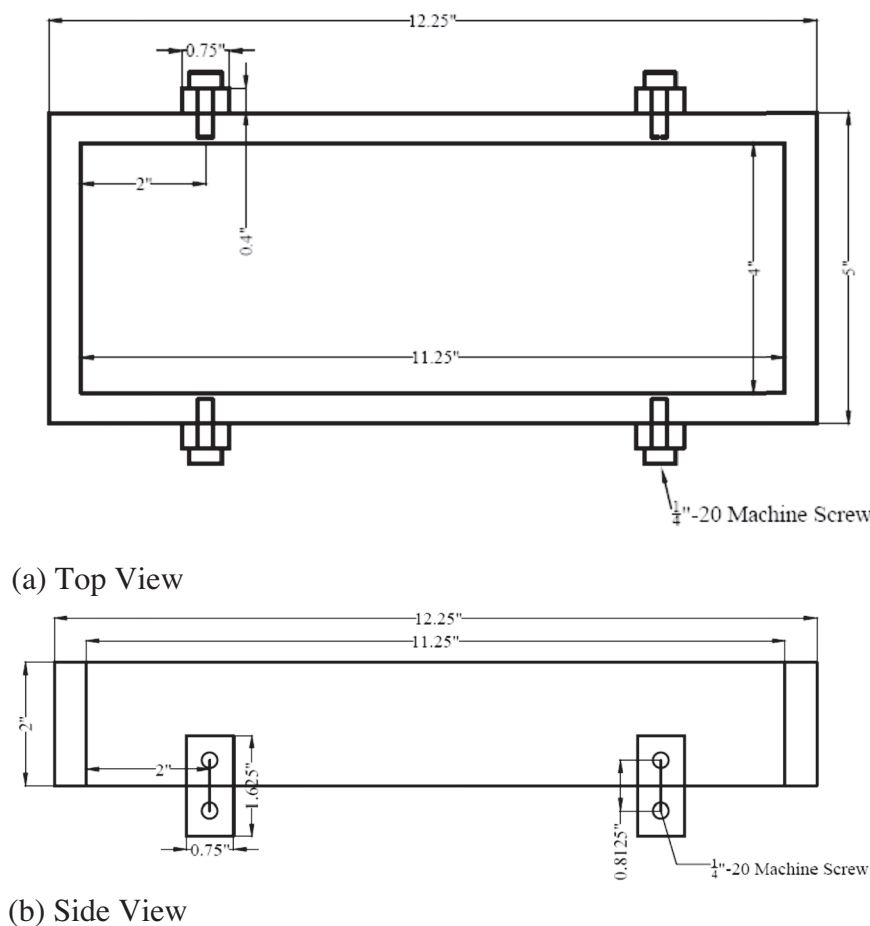
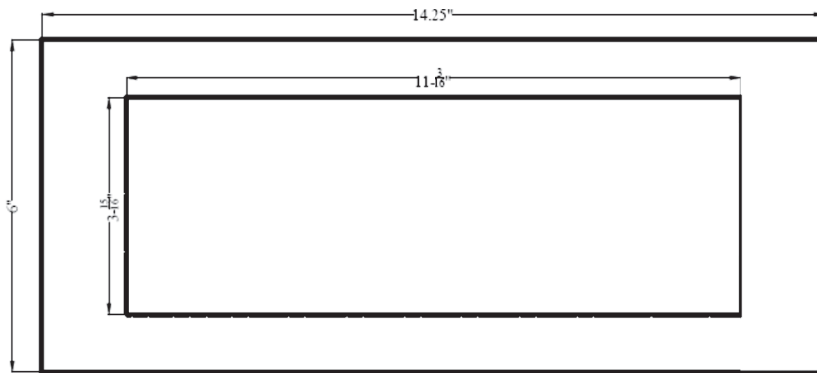
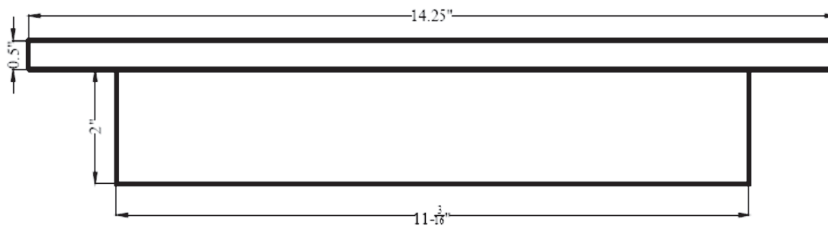


Figure 1—Extension Collar

- 5.2. *Top Plate*—A 50.8 mm (2 in.) tall steel plate with a cap should fit in the extension collar and have a flat bottom surface. The top plate shall be constructed as shown in Figure 2.



(a) Top View



(b) Side View

Figure 2—Top Plate

- 5.3. *Gauge*—A linear variable differential transformer (LVDT) gauge head with excitation source and digital readout, with a minimum resolution of 0.00025 mm (0.00001 in.), and a range suitable for the test [for ease in setting up the apparatus, a range of ± 2.5 mm (0.1 in.) has been found practical] (Note 1).

Note 1—LVDT with the appropriate associated electronic actuating and indicating apparatus appears to give the best results with respect to stability, sensitivity, and reliability. Multichannel recording of outputs has been found to be practical and efficient. As an alternative, a data logger can be used to excite the LVDT and record the LVDT and both temperature and time outputs. The data can be stored directly in a personal computer for graphing of test results.

- 5.4. *Temperature-Measuring Devices*—Two temperature-measuring devices with a resolution of 0.1°C (0.2°F) and accurate to 0.2°C (0.4°F). T-Type thermal couple has been found to be suitable for this measurement.
- 5.5. *Dial Gauge Mount*—Dial gauge mount shall support the LVDT and be glued onto the specimen directly.
- 5.6. *Balance*—A scale or balance having a capacity of 10 kg (22 lb) and accurate to 0.1% over its range.

- 5.7. *Mixing Tools*—Miscellaneous tools such as a mixing pan, spoon, trowel, spatula, etc. or a suitable mechanical device for thoroughly mixing the sample of soil with increments of water.
- 5.8. *Containers*—Suitable containers made of material resistant to corrosion and not subject to change in mass or disintegration on repeated using.
- 5.9. *Compactor*—A compactor with enough power to obtain target density of specimen.
- 5.10. *Stainless Steel or Aluminum Plates*—Two stainless steel or aluminum plates should have smooth surface with dimension large enough to hold the specimen (101.6 mm × 285.75 mm or 4 in. × 11.25 in.).
- 5.11. *Environmental Chamber*—An environmental chamber capable of applying variable temperature and humidity cycles without shock, and these cycles shall meet the specific test condition. Specimens shall be stored horizontally with suitable racks. The racks shall be positioned such that the air circulation is not disturbed or restricted in the intervening space.

6. TEST SPECIMENS

- 6.1. Determine the optimum moisture content and maximum dry density of the material in accordance with ASTM D 698; except when the 152.4 mm (6 in.) mold is used, the rammer shall weigh 4.54 kg (10 lb) and the vertical drop distance shall be 457 mm (18 in.).
- 6.2. Calculate the total mass of mixture needed based on the maximum dry density, and add soil and required additive and water in the container.
- 6.3. Add to the soil in the container the required amount of cementitious additive. Mix the soil and additive thoroughly until color of the mixture is uniform.
- 6.4. Add potable water to reach the optimum moisture content and mix thoroughly.
- 6.5. Tape a thin layer of plastic, no more than 0.0254 mm (0.001 in.) thickness, inside the mold, in order to prevent the bonding between specimen and steel mold during compaction.
- 6.6. After imbedding the tip of the thermal couple at center of the mold, transfer the calculated mass of the mixture into the mold. If the mold is not big enough to hold the loose material, push the mixture with the top plate, until all the material is moved into the mold. Make sure the uncompacted mixture has uniform height.
- 6.7. Compact the specimen with the air rammer carefully. Check the height of the specimen during compaction until it is close to the target height. Then put the top

plate (Figure 2) on the mold and continue compaction until the top plate touches the mold.

- 6.8. Demold the specimen. Take apart the extension collar and four sides of the mold first. Then put a steel plate on the side of the specimen, hold the bottom plate of the mold and the steel plate, and flip the specimen 90°. Now the specimen is held by the steel plate. Replace the bottom plate of the mold with another steel plate and flip the specimen 90° in the opposite direction. After that, the specimen is transferred from the mold to the steel plate.
- 6.9. Glue the gauge mount with quick-setting epoxy onto the specimen and make sure the LVDT measures the longitudinal axis of the specimen.
- 6.10. Move the specimen to the environmental chamber. Adjust the position of the LVDT tip to the midpoint of the entire range.
- 6.11. Place another thermal couple to collect chamber temperature during test. Connect the imbedded thermal couple and the ambient-temperature thermal couple to a data acquisition device.

7. PROCEDURE

- 7.1. Place the specimen in the environmental chamber at an initial ambient temperature of 25°C until the temperature inside the specimen is uniform. The chamber shall start to cycle the temperature between 25°C and 30°C using a saw-tooth pattern with constant relative humidity. After the target temperature in the chamber is reached, which takes about 20 min, the temperature shall be kept constant for 4 hours, resulting in three full cycles (or six steps) per day. The constant temperature period is long enough to ensure a stable and uniformly distributed temperature in the prism specimen. The amplitude of the temperature cycle (5°C) is selected to be small enough to maximize the number of cycles per day and obtain more COTE values at early ages, and can minimize the temperature effect on the change in COTE over time.

8. CALCULATION

- 8.1. Calculate the strain at any age as follows:

$$\varepsilon = \left(\frac{L_x - L_i}{L} \right) \times 10 \quad (I)$$

where:

ε = strain in length at x age, percentage;

L = initial specimen length, mm (in.);

L_x = LVDT reading at x age, mm (in.); and

L_i = initial LVDT reading, mm (in.);

- 8.2. Calculate the coefficient of thermal expansion as follow (Note 2):

$$\text{COTE} = \frac{(\Delta\varepsilon_{\max} - \Delta\varepsilon_{\min})}{\Delta T} + \alpha' \quad (2)$$

where:

$\Delta\varepsilon_{\max}$ = maximum strain in each step;

$\Delta\varepsilon_{\min}$ = minimum strain in each step;

ΔT = the incremental change in temperature, 5°C in this case; and

α' = the COTE of LVDT, obtained from LVDT specifications.

Note 2 – When plotting the development of COTE with time, the COTE shall be the average COTE in each cycle, including both temperature increase and decrease steps. It is suggested to calculate the COTE starting when the temperatures from imbedded and air-temperature thermal couples are close.

- 8.3. Calculate strain values for each specimen to the nearest 10^{-6} and report averages to the nearest 10^{-5} and COTE to the nearest 10^{-6} .

9. REPORT

- 9.1. *Report the following information:*

- 9.1.1. Identification of types of host material and additive, number of specimens for each condition, and date & place molded;
- 9.1.2. Source and identification of each material employed;
- 9.1.3. Type, maximum size, moisture condition, and grading of the soil;
- 9.1.4. Size of specimens;
- 9.1.5. Mixture proportions, including additive content, optimum moisture content, and maximum dry density;
- 9.1.6. Description of environmental condition, including temperature and humidity collected during the test;
- 9.1.7. Total elapsed time while recording readings;

- 9.1.8. Length change data, reported as strain, either increase or decrease in linear dimension, to the nearest 10^{-6} of the length based on the initial measurement at the time of placing the LVDT on the specimen;
- 9.1.9. Technician conducting test; and
- 9.1.10. Any other pertinent information.

10. PRECISION AND BIAS

- 10.1. *Precision*—No precision data are available using this test method.
- 10.2. *Bias*—No bias can be established because no reference material is available for this test.

11. KEYWORDS

- 11.1 Coefficient of thermal expansion (COTE); cementitiously stabilized materials; soil stabilization.

12. REFERENCES

- 12.1. Cusson, D. and T. J. Hoogeveen. 2006. Measuring Early-Age Coefficient of Thermal Expansion in High-Performance Concrete. *International RILEM Conference on Volume Changes of Hardening Concrete: Testing and Mitigation*, Lyngby, Denmark, August 20.

Proposed Standard Method of Test for

Shear Strength Test of Cementitiously Stabilized Soils

Designation:

Other Standard Designation: Iowa 406-C-2000

1. SCOPE

- 1.1. This test method covers determination of the shearing strength of cementitiously stabilized soil.
- 1.2. The values stated in SI units are to be regarded as the standard. The English unit equivalents shown in parentheses may be appropriate, except with regard to sieve sizes and aggregate size as determined by the use of testing sieves, in which case the standard SI designation shown is the standard as required by AASHTO Specification M 92.
- 1.3. This standard may involve hazardous materials, operations, and equipment. This standard does not purport to address all of the safety problems associated with its use. It is the responsibility of the user of this standard to establish appropriate safety and health practices and determine the applicability of regulatory limitations prior to use.

2. DEFINITIONS

- 2.1. The definitions of “cementitiously stabilized soils” are any types of soils (gravel, sand, silt, or clay) stabilized by cementitious additives (cement, lime, fly ash, or any combination of them).
- 2.2. The term “shear strength,” as used in this specification, is defined as the maximum load carried by the specimen during the test divided by the cross-sectional area. The term “coefficient of friction,” as used in this specification, is defined as slope of shear stress and displacement in direct shear test of cementitiously stabilized soil. The coefficient of friction can be used as an input value for the restrained shrinkage cracking model.

3. REFERENCED DOCUMENTS

3.1. *AASHTO Standards:*

- M 92, Wire-Cloth Sieves for Testing Purposes
- T 180, Moisture–Density Relations of Soils Using a 4.54 kg (10 lb) Rammer and a 457 mm (18 in.) Drop

3.2. *ASTM Standards:*

- D 698, Standard Test Methods for Laboratory Compaction Characteristics of Soil Using Standard Effort
- D 2166, Standard Test Method for Unconfined Compressive Strength of Cohesive Soil

3.3. *Other Standard:*

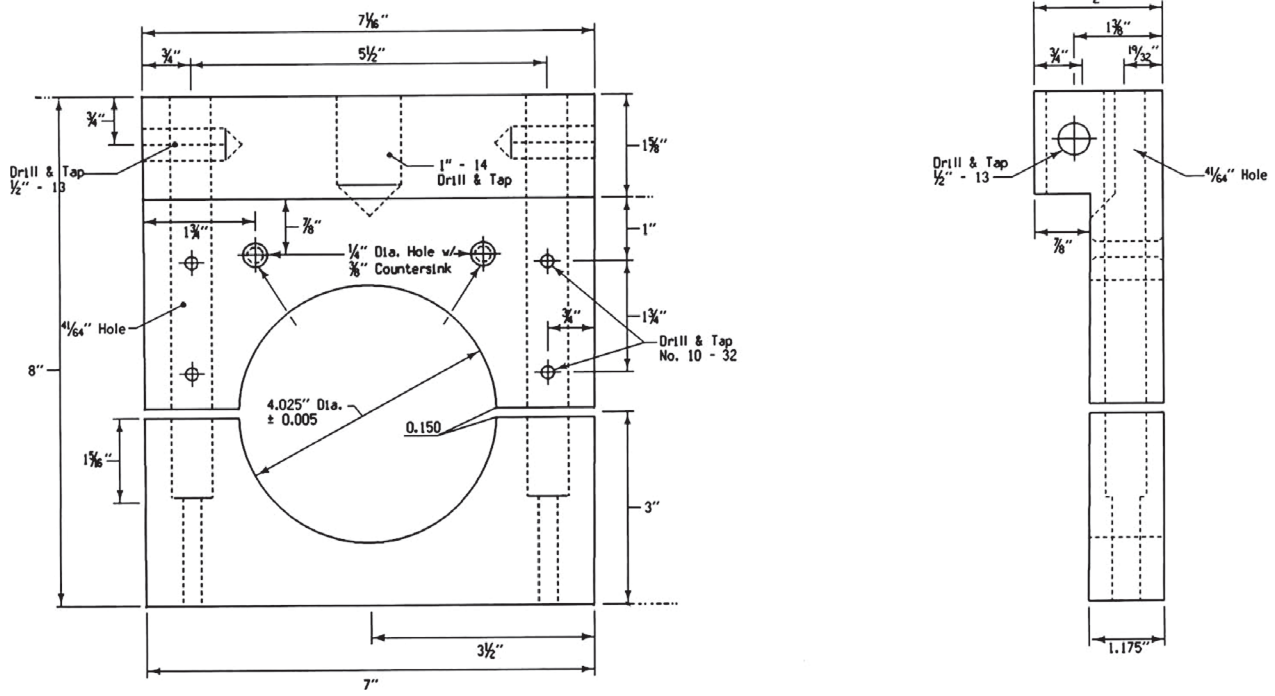
- Iowa 406-C, Method of Test for Determining the Shearing Strength of Bonded Concrete

4. SIGNIFICANCE AND USE

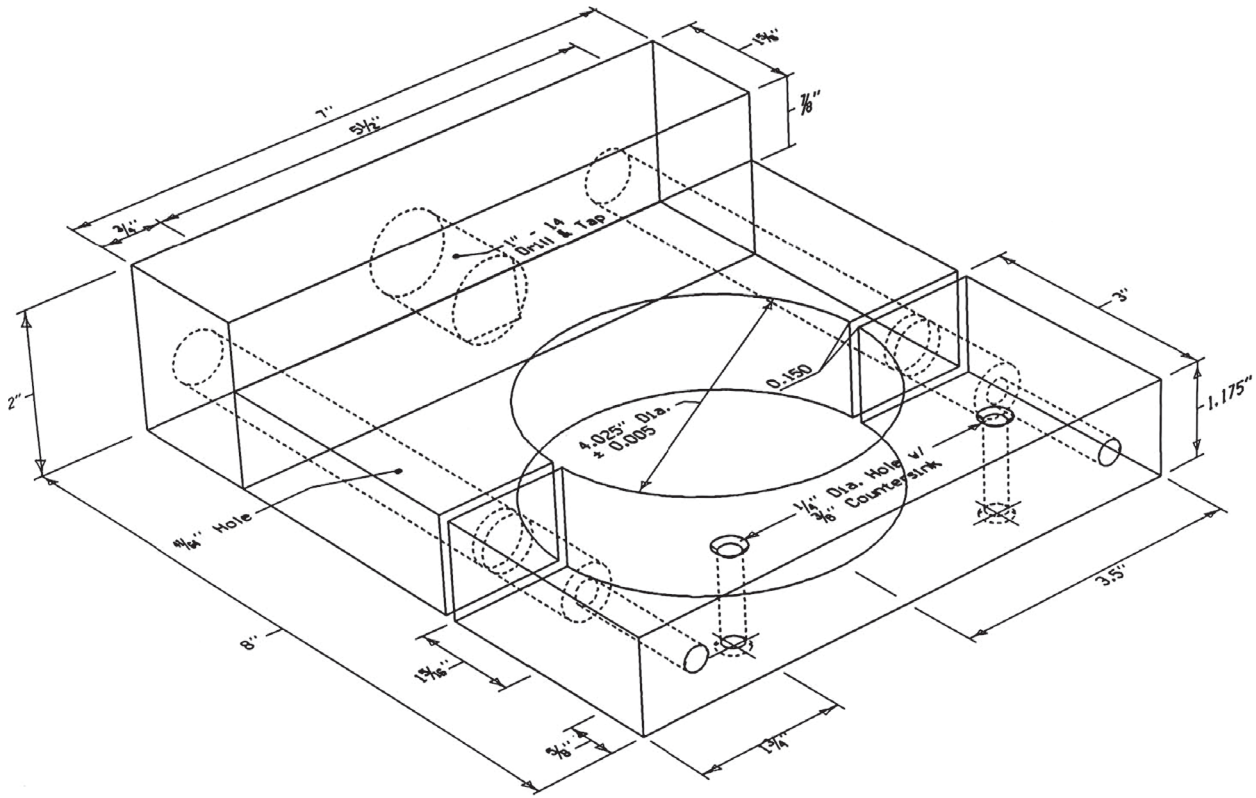
- 4.1. This practice is intended to provide standard requirements for apparatus common to many test methods used in connection with cementitiously stabilized soils and standardized procedures for its use. The detailed requirements as to materials, mixtures, specimens, conditioning of specimens, number of specimens, ages at which measurements are to be made, interpretation of results, and precision and bias are left to be dealt with in specific test methods.

5. APPARATUS

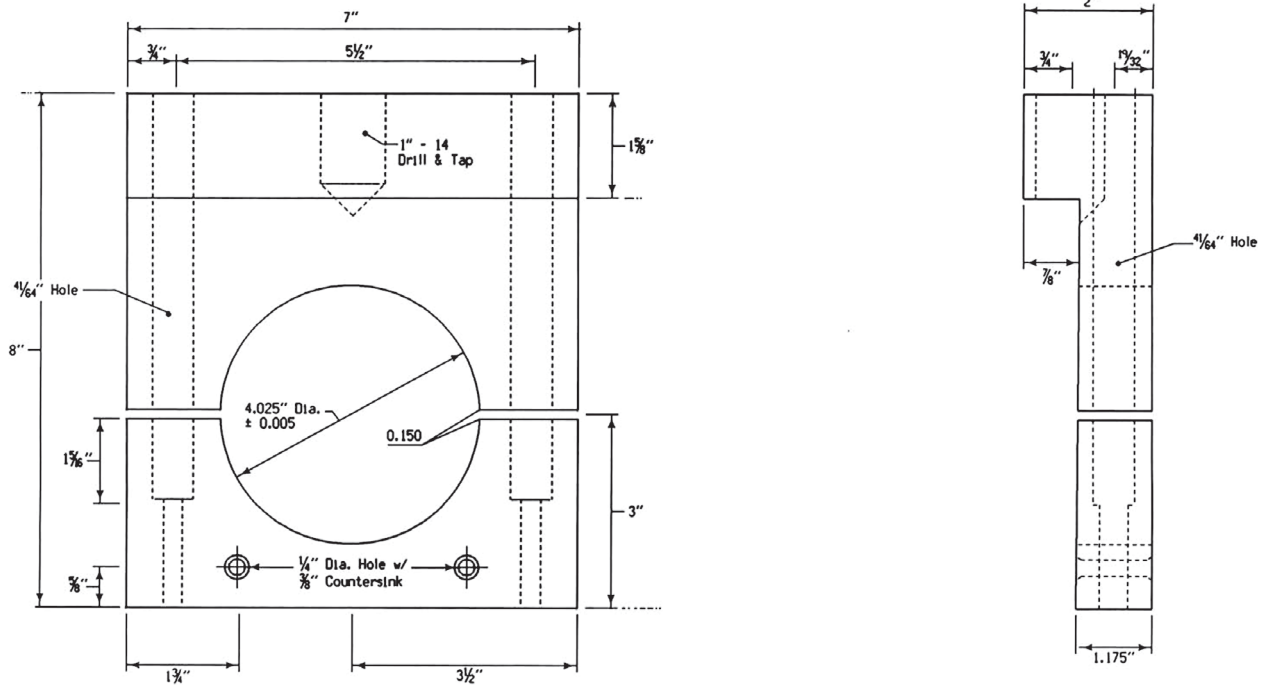
- 5.1. *Testing Jig*—The testing jig shall accommodate a 101.6 mm (4 in.) diameter specimen. The jig is designed to provide a direct shearing force along the cross section. The testing jig shall be constructed as shown in Figure 1.



(a) Side View
Figure 1-Testing Jig

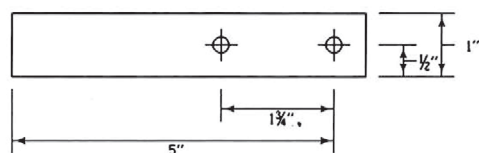
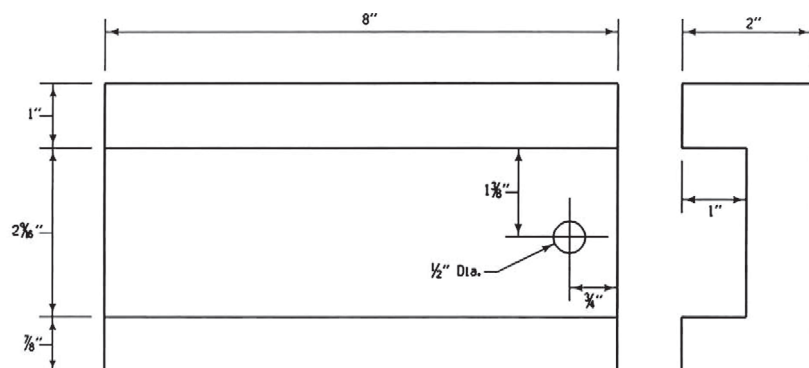


(b) 3-D View



(c) Side View

Figure 1—Testing Jig (continued)



(d) Side View

Figure 1-Testing Jig (continued)

- 5.2. *Hydraulic Testing Machine*—The hydraulic testing machine shall be capable of applying a smooth and uniform load. The accuracy of the reading shall be within $\pm 1.0\%$ of the indicated load.
- 5.3. *Displacement-Measuring Device*—Device capable of recording displacement continuously. Linear Variable Differential Transformer (LVDT) with a range of at least 5 mm and linearity error smaller than $\pm 0.25\%$ is recommended, for measurement of slippage displacement.
- 5.4. *Specimen Dimension Measurement Devices*—Dial comparators, calipers, circumferential tape, or other suitable devices for measuring the height and diameter of the specimen to three significant digits.
- 5.5. *Specimen Mold*—Molds with 101.6 mm (4 in.) diameter for Proctor compaction test conforming to the requirements of ASTM D 698.
- 5.6. *Balance*—A scale or balance having a capacity of 10 kg (22 lb) and accurate to 0.1% over its range.
- 5.7. *Mixing Tools*—Miscellaneous tools such as a mixing pan, spoon, trowel, spatula, etc. or a suitable mechanical device for thoroughly mixing the sample of soil with increments of water.

- 5.8. *Containers*—Suitable plastic airtight, moisture-proof containers for sealing and storing specimens after compaction. The containers should be rigid to protect the specimens from disturbance during handling.
- 5.9. *Tamping Rod or Compaction Rammer*—Tamping rod or compaction rammer suitable for mold size and preparation of specimen at desired unit weight.
- 5.10. *Test Specimen Extruder*—An extruder is required if split molds are not used. The device shall consist of a piston, jack, and a frame or similar equipment suitable for extruding specimens from the mold.
- 5.11. *Temperature-Controlled Room or Cabinet*—A room or cabinet capable of maintaining a temperature of $23\pm 2^{\circ}\text{C}$ ($73\pm 4^{\circ}\text{F}$) for curing specimens. A moist room can be used but is not required.

6. PROCEDURE

- 6.1. Obtain the optimum moisture content and maximum dry density according to ASTM D 698; except when the 152.4 mm (6 in.) mold is adopted, the rammer shall weigh 4.54 kg (10 lb) and the vertical drop distance shall be 457 mm (18 in.).
- 6.2. Prepare specimens to the predetermined water content and target dry density with 101.6 mm (4 in.) mold. After a specimen is formed, trim the ends perpendicular to the longitudinal axis (Note 1), remove from the mold, and determine the mass and the dimensions of the test specimen.

Note 1—Flat end can be obtained by compacting the last layer on a flat plate with a cap.

- 6.3. After the mass and dimensions of the specimen have been determined, place the specimen in an airtight, moisture-proof container and allow the specimen to cure at a temperature of $23\pm 2^{\circ}\text{C}$ ($73\pm 4^{\circ}\text{F}$) for the specified curing period (Note 2).

Note 2—Any curing period may be specified; however, the most commonly used curing periods are 7, 28, and 90 days.

- 6.4. When running the shear strength test, place the specimen in the testing jig in such a manner that the cross section of the specimen is parallel to the moving direction of the main halves of the jig (Note 3).

Note 3—In the event that the interface is irregular and cannot entirely be placed within the specified space, the interface will be placed as close as practical and a special notation made.

- 6.5. Carefully align the testing jig in the testing machine with the central axis of the jig in the center of the testing machine.
- 6.6. Apply the load continuously and without shock so as to produce an axial deformation rate of $15\% \pm 2.0\%$ per minute.

- 6.7. Continue the loading until the specimen fails, and record the stress carried by the specimen and related displacement during the test.

7. CALCULATION OF LENGTH CHANGE

- 7.1. Calculate the shear strength of the specimen as the maximum load carried by the specimen during the test divided by the cross-sectional area and express the result to the nearest MPa (psi); and calculate the coefficient of friction as the slope by plotting the shear stress and displacement curve, and express the result as MPa/mm (psi/in.).

8. REPORT

- 8.1. The report shall include the following:
- 8.1.1. Identification as types of host material and additive, number of specimens for each condition, and date & place molded;
 - 8.1.2. Source and identification of each material employed;
 - 8.1.3. Type, maximum size, moisture condition, and grading of the soil;
 - 8.1.4. Size of specimens;
 - 8.1.5. Mixture proportions, including additive content, optimum moisture content, and maximum dry density;
 - 8.1.6. Description of curing condition, including temperature and humidity;
 - 8.1.7. Deformation rate, load and displacement during the test, elapsed time since the start of loading.
 - 8.1.8. Technician conducting test; and
 - 8.1.9. Any other pertinent information.

9. PRECISION AND BIAS

- 9.1. *Precision*—No precision data are available using this test method.
- 9.2. *Bias*—No bias can be established because no reference material is available for this test.

10. KEYWORDS

- 10.1 Shear strength; coefficient of friction; cementitiously stabilized materials; soil stabilization.

APPENDICES

Appendixes A through F contained in the research agency's final report provide elaborations and detail on several aspects of the research; they are not published herein but are available by searching for *NCHRP Report 789* on the TRB website (www.TRB.org). These appendixes are:

- A: Literature Review and Survey Results
 - B: Mix Design and Test Procedure Evaluation
 - C: Development of Experiments and Findings for Distress Models
 - D: FWD Backcalculation Error Analysis
 - E: Reasonableness Analysis of Field-Calibrated Models
 - F: Bibliography
-

Abbreviations and acronyms used without definitions in TRB publications:

A4A	Airlines for America
AAAAE	American Association of Airport Executives
AASHO	American Association of State Highway Officials
AASHTO	American Association of State Highway and Transportation Officials
ACI-NA	Airports Council International-North America
ACRP	Airport Cooperative Research Program
ADA	Americans with Disabilities Act
APTA	American Public Transportation Association
ASCE	American Society of Civil Engineers
ASME	American Society of Mechanical Engineers
ASTM	American Society for Testing and Materials
ATA	American Trucking Associations
CTAA	Community Transportation Association of America
CTBSSP	Commercial Truck and Bus Safety Synthesis Program
DHS	Department of Homeland Security
DOE	Department of Energy
EPA	Environmental Protection Agency
FAA	Federal Aviation Administration
FHWA	Federal Highway Administration
FMCSA	Federal Motor Carrier Safety Administration
FRA	Federal Railroad Administration
FTA	Federal Transit Administration
HMCRP	Hazardous Materials Cooperative Research Program
IEEE	Institute of Electrical and Electronics Engineers
ISTEA	Intermodal Surface Transportation Efficiency Act of 1991
ITE	Institute of Transportation Engineers
MAP-21	Moving Ahead for Progress in the 21st Century Act (2012)
NASA	National Aeronautics and Space Administration
NASAO	National Association of State Aviation Officials
NCFRP	National Cooperative Freight Research Program
NCHRP	National Cooperative Highway Research Program
NHTSA	National Highway Traffic Safety Administration
NTSB	National Transportation Safety Board
PHMSA	Pipeline and Hazardous Materials Safety Administration
RITA	Research and Innovative Technology Administration
SAE	Society of Automotive Engineers
SAFETEA-LU	Safe, Accountable, Flexible, Efficient Transportation Equity Act: A Legacy for Users (2005)
TCRP	Transit Cooperative Research Program
TEA-21	Transportation Equity Act for the 21st Century (1998)
TRB	Transportation Research Board
TSA	Transportation Security Administration
U.S.DOT	United States Department of Transportation